CHALMERS

Dynamic response of a transition zone on soft clay

JELKE DIJKSTRA & HOSSEIN TAHERSHAMSI

Department of Architecture and Civil Engineering
Geology & Geotechnics
CHALMERS UNIVERSITY OF TECHNOLOGY
Göteborg, Sweden 2020

TECHNICAL REPORT GEOTECHNICAL ENGINEERING

Dynamic response of a transition zone on soft clay

JELKE DIJKSTRA & HOSSEIN TAHERSHAMSI

Department of Architecture and Civil Engineering
Geology & Geotechnics
CHALMERS UNIVERSITY OF TECHNOLOGY
Göteborg, Sweden 2020

Dynamic response of a transition zone on soft clay
JELKE DIJKSTRA & HOSSEIN TAHERSHAMSI
ISBN xxx

Technical report 2020:AUG21
ISSN xxx-xxx
Department of Architecture and Civil Engineering
Geology & Geotechnics
Chalmers University of Technology
SE-412 96 Göteborg
Sweden
Telephone: +46 (0)31-772 2120

Chalmers Reproservice
Göteborg, Sweden 2020

Dynamic response of a transition zone on soft clay
Technical report Geotechnical Engineering
JELKE DIJKSTRA & HOSSEIN TAHERSHAMSI
Department of Architecture and Civil Engineering
Geology & Geotechnics
Chalmers University of Technology

Abstract

This report for project *TRV 2016/106277* presents the development of numerical methods to study the effect of strain accumulation from cyclic loading on the dynamic response of a railway system. The work is a follow up on the project *TRV 2015/108250 – Modelling deformations below high-speed rail*. The following advances are made, which are in line with the recommendations of the previous project:

- Stiffness degradation based on experimental data is implemented in the constitutive model for cyclic accumulation of strain in soft soils: Creep-Sclay1Sc;
- The boundary value level analyses are now considering 2D longitudinal sections with moving train loads;
- The analyses now incorporate quasi-static cyclic accumulation modelling and time-domain dynamic analyses for a single train passage before and after simulating 100 000 load cycles.

Subsequently a transition zone is studied numerically where an embankment is overlaying a soft clay that is prone to settlements from cyclic loading and a competent stiff soil. The train loads are simulated by moving four spring loaded point loads (one for each axle), which required some changes in the *Tochnog Professional* Finite Element code. Special care was taken to convert the characteristics of the dynamic load to appropriate input parameters for the cyclic accumulation model. It is demonstrated that for the boundary value problem considered the period for cyclic loading in the soft clay below the embankment is associated to the distance between the bogeys. Furthermore, the maximum deviatoric stress amplitude reduces with depth rather quickly.

The transition zone is studied for axle loads of 60 kN spaced following the X2000 passenger carriage configuration for two train velocities, i.e. $10\,\mathrm{m\,s^{-1}}$ and $50\,\mathrm{m\,s^{-1}}$ using the cyclic strain accumulation model with and without stiffness degradation. The results indicate that the second train passage after cyclic degradation resulted in lower induced stress amplitudes, for both models. The effect of the stiffness degradation linked to destructuration in the clay is limited for the studied cases where the deviatoric loading amplitude for cyclic accumulation was modest. Larger values for the deviatoric loading amplitude proved to be leading to numerical stabilities issues.

The measurable project impact is itemised below:

- Improved constitutive model for strain accumulation of soft sensitive clay;
- The resulting analysis method will be used in the follow up project in conjunction with the sensitivity analyses framework;
- All calculations can be performed with the *Tochnog Professional* Finite Element code, which since January 2020 is free to use for all. This dramatically improves market adaptation.

Keywords: strain accumulation, time effects, high-speed rail, soft soils, transition zones

Contents

1 Introduction

1.1 Background

Problem origin

In most (high-speed, HS) line infrastructure, very strict alignment and stiffness variations are prescribed. These perhaps result in overly costly track configurations being pre-scribed to prevent additional maintenance issues resulting from track degradation down the line. At present the complete system of railway head, sleepers, subgrade (slab), embankment and subsoil are not considered in setting these guide lines. The subsoil (and embankment) will have a profound effect on the dynamic track response. Both positively (redistributing the load, attenuation of energy) and negatively (on-going settlements from consolidation and creep that is accelerated by track operation). It, therefore, would be prudent to investigate the impact of the evolving stiffness in the subsoil that results from cyclic loading on the emerging dynamic response at the top of the railway system. This project focuses on investigating a simplified system with a transition from a soft soil with a low stiffness that is prone to further degradation to a stiff soil.

Traditional modelling strategies for transition zones

Most rail track-bed modelling strategies only consider the dynamic response of the track-ballast and subgrade without incorporating the response of the deeper soil layers, also totally ignoring effects of groundwater. Most notably the models developed in Sweden, e.g. by CHARMEC researchers focus on advanced wheel-rail interaction models with simplified models for the ballast, subballast and subgrade (e.g. Nielsen and Li 2018). These somewhat crude modeols for the railway foundation system have been extended in order to incorporate permanent settlements, primarily in the ballast (Sato 1997; Dahlberg 2001). More extensive Finite Element Analyses have also been presented by numerous authors, however, in those the focus was on the dynamic response of the stiffness transition and not the role of consolidation and creep processes in the subsoil. Coelho et al. (2011) and Zuada Coelho and Hicks (2016) shows that time domain Finite Element analyses are helpful in studying those issues with a focus on the role of the subsoil. More recently, Li et al. (2016) used the cyclic accumulation model originally developed by (Suiker and Borst 2003) to study settlements in the ballast below railway turn outs. Still, the effect of the degradation of the properties in the subsoil still needs to be explicitly incorporated in the study of transition zones. Furthermore, the unloaded track level has a an impact on the force that is transferred to the subsoil , as such permanent changes in level of should be part of the analyses (e.g. Powrie et al. 2019).

Strain accumulation models for ballast and soils

When complex constitutive models, specifically designed to truthfully capture each loading cycle (e.g. those inspired by the work of Mrŏz et al. 1978), are used to solve cyclic problems with a large number of loading cycles, $O(10^5)$, issues related to the computational cost and numerical convergence arise. In order to overcome these difficulties, several authors have developed cumulative degradation models to account for the effects of cyclic plastic strains of a large number of loading cycles (Karg et al. 2010; Li et al. 2016; Ni et al. 2014; Niemunis

et al. 2005; Pasten et al. 2014; Suiker and Borst 2003). With exception of the work of Ni et al. (2014), all the existing models were developed for coarse grained granular materials. Therefore, there is a lack of models suitable for simulating soft soils. The main limitation of the model presented by Ni et al. (2014) is that it ignores fundamental soft soil features,such as rate-dependency, anisotropy and degradation of bonding (Karstunen et al. 2005; Leroueil and Vaughan 1990; Wheeler et al. 2003). This project aims to address these limitations by developing an accumulation model for soft sensitive clays.

Finally, the new constitutive model, Creep-Sclay1Sc which is an extension on the Creep-Sclay1S model (Sivasithamparam et al. 2015; Gras et al. 2017) developed in the prior project can be considered the most comprehensive accumulation model for soft soils. The model, however, does not explicitly incorporate stiffness degradation in the pseudo-elastic range, i.e. stress states that fall below the pre-consolidation pressure.

1.2 Aim

This project will investigate numerically the evolving complex (frequency and amplitude dependent) stiffness response of a soft clay near a transition to a stiff soil (subgrade)[1].

1.3 Objectives

- Adding stiffness degradation to the constitutive model for cyclic loading of sensitive clay;
- Combining quasi-static strain accumulation modelling with time domain dynamic Finite Element analyses;
- Analyses of the role of cyclic accumulation of 2D longitudinal cross section for a moving train load.

1.4 Limitations

- A simplified problem geometry without explicitly modelling the track system will be studied, i.e. an embankment overlaying two soil types.

[1]Note that this objective is somewhat adapted from the original project proposal to better align the activities within the highspeed rail research projects at Chalmers.

2 Methodology

2.1 Introduction

This Chapter presents some numerical modelling details that needed to be developed for the analyses presented herein. In addition to a modification of the cyclic accumulation model Creep-SClay1Sc for the degradation of the 'pseudo-elastic' (small strain) stiffness the FE code adopted was altered to interpolate moving loads between nodes in the mesh, and some guidance on how the dynamic analyses on moving loads informs the model parameters in the pseudo-static accumulation model.

2.2 Adding stiffness degradation to Creep-SClay1Sc

2.2.1 Experimental evidence

Wood (2016) presents some data on the evolution of shear wave velocities V obtained with bender elements during monotonic undrained shearing of samples of sensitive Swedish clay in a triaxial test. The results are normalised with the initial reading of the shear wave velocity V_0 prior to shearing and re-plotted against the globally measured axial strain in Figure 2.1.

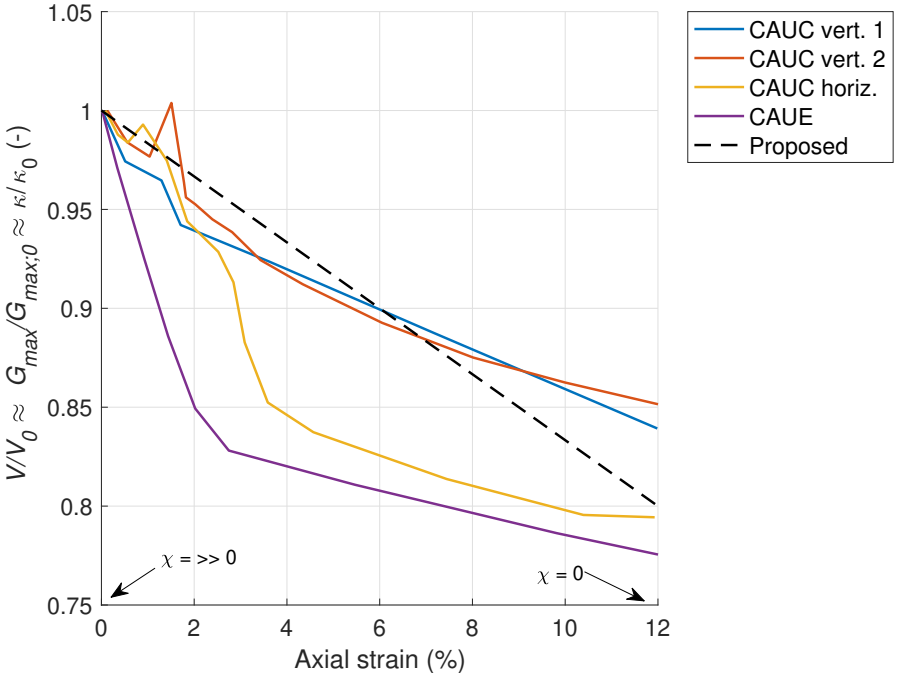

Figure 2.1: *Reduction in shear wave velocities during undrained shearing in an anisotropically consolidated sample of a Swedish sensitive clay; CAUC = compression; CAUE is extension; horiz: is horizontally cut sample. Reworked from Wood (2016).*

A main observation is that the shear wave velocities reduce up to 20% during axial straining. The largest degradation in shear wave velocities is observed for samples that are sheared in a significantly different loading direction, i.e. extension; horizontally oriented sample. For these loading paths the micro-structure that governs the small-strain stiffness is changing

most rapidly. It is postulated that a similar limiting small-strain stiffness is reached for the vertically oriented and loaded samples, only at larger magnitudes for axial strain. As such a linear relation is proposed, and plotted in Figure 2.1, that reduces the intact stiffness to 0.8 of its original magnitude at large magnitudes of strain. In the model this is best linked to the destructuration parameter χ.

2.2.2 Implementation

The stiffness degradation is implemented without resorting to fully reformulating the hardening laws in the model and/or adding additional elastic bubbles (as is done in bounding surface models). Rather a dependency of the input parameter that controls the stiffness in the pseudo-elastic regime is used, which for the cyclic accumulation model Creep-SClay1Sc model is κ. The data on shear wave velocities suggests a reduction in stiffness at small strain amplitudes as function of axial strain during undrained triaxial testing. Although this small-strain stiffness cannot be directly compared to the global stiffness response of element level tests (i.e. the reduction in the stress/strain ratio observed) it is a more accurate description of the stiffness response under dynamic train loading. It is postulated that the physical interpretation of the stiffness degradation is linked to the bonding (structure) in sensitive clays.

With increased global strains the destructuration in the material will destroy all bonds which results in altered inter-particle response at small strain. As such the reduction of the shear wave velocities, hence the shear modulus G and bulk modulus, at large levels of global strain ($> 12\%$) observed experimentally is linearly linked to the model parameter χ. χ controls the degree of destructuration in the cyclic accumulation model. For intact clays represented by $\chi_0 >> 0$ in the model an initial value for κ_0 will be used whilst after plastic straining (e.g. from accumulated settlements) the χ approximates 0 and κ will be a reduction factor r times κ_0. This conveniently enables an irreversible stiffness degradation that is anisotropic and is only linked to (large) plastic strains for which the data is obtained. Furthermore, in the model the destructuration of χ_0 will be less rapid than for extension in a similar way as it is observed in the data.

After some re-arrangements the relation implemented reads:

$$\kappa = \kappa_0 \left[(1 - r) \frac{\chi}{\chi_0} + r \right] \tag{2.1}$$

The choice to degrade κ in a similar manner as is observed for the shear modulus G in the experimental data is reasonable. The behaviour of the bulk modulus in the pseudo-elastic range is uniquely linked to the shear modulus with the Poisson ratio. The limited availability of experimental data does not inform a more refined relationship that explicitly incorporates this relation in more detail. Furthermore, varying the stiffness in-between calculation steps is numerically challenging, as in each subsequent calculation step the stress field at the start of the iteration is not in equilibrium with the stiffness properties which have been updated since equilibrium was reached.

Finally, taking into consideration the data available and the theoretical relation established, only one model parameter needs to be added, i.e. r which is set at $r = 0.8$ in all calculations with stiffness degradation enabled.

2.3 Modelling moving train loads

2.3.1 Moving boundary conditions

The *Tochnog Professional* Finite Element code used for the analyses allows for great flexibility to apply and update boundary conditions (BCs). A typical approach is to define a geometry entity in the model for which the BCs are set. Subsequently, internally during the calculations, all nodes that fall within the geometry entity (point, line, surface or volume in space, depending on the number of dimensions required in the analyses) plus an additional tolerance will get these BCs prescribed. *Tochnog Professional* updates the location of the BC when nodes move, e.g. in an Update Lagrangian spatial formulation, or alternatively when the user prescribe a change in the location of the geometry entity. This approach has been successfully used to model pile installation and moving train loads (Dijkstra et al. 2011; Zuada Coelho and Hicks 2016). For a moving train load this would imply that a geometry line with length L_a with a distributed load q_a prescribed can be moved along the surface of the modelled embankment (Fig. 2.2). As soon as the nodes of an element fall below this geometry entity, i.e. within the influence radius r_L, they will receive (part) of the distributed load. For this modelling approach to work reliably, the geometry line should cover at least 10 nodes, which requires a large number of (small) elements in case the contact area is small.

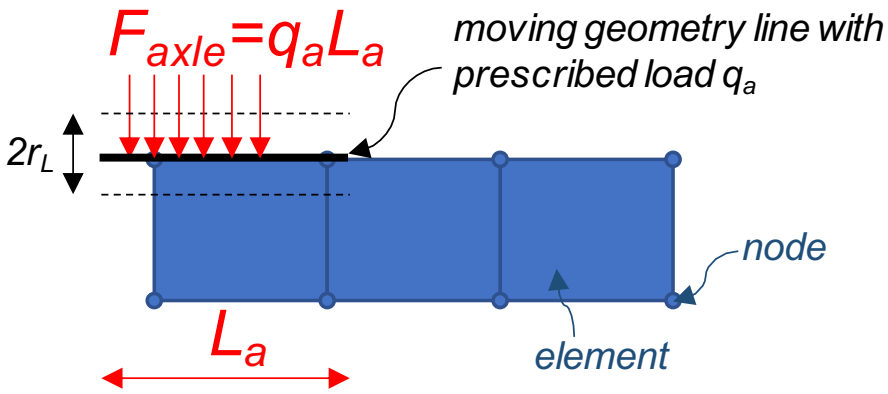

Figure 2.2: *Numerical modelling approach for moving axle loads in FE analysis; The geometry line with length L and influence radius r_L has a distributed load q_L prescribed as BC. This geometry entity is moved with the train velocity.*

During initial trial calculations, the results indicated issues with the interpolation of the load when the element size in the domain was relatively large compared to the size of the contact area. Quite often the moving BC would not activate any nodal forces and only after tedious optimisation of all relevant numerical details (mesh size, time step size, prescribed train velocities, size of contact area) a reasonable result can be obtained for the train passage prior to cyclic accumulation. However, after settlements of the top of the embankment the load would not be in contact with the nodes in case the settlements exceed the r_L, and the whole optimisation process starts again.

Taking these complications into consideration this approach was abandoned for a more robust method where for each axle a 2D spring element is generated, and subsequently moved. This approach is described in the next Section.

2.3.2 Spring elements and multipoint constraints

An alternative method for prescribing the moving axle loads of a passing train in *Tochnog Professional* has been developed in conjunction with the developer. The approach revolves around enabling the interaction of two parts of the mesh or two separate mesh entities that initially are not connected via multipoint constraints -mpc-. An mpc links a principal degree of freedom (e.g. displacements, velocities) between the two mesh entities and takes care of the relative positions of the nodes, and interpolates where necessary. As such the interactions are continuously updated and the load applied smoothly in space. In the current approach the vertical component of the velocities is used in the mpc. Figure 2.3 shows a sketch of the approach. The axle load F_{axle} is transferred with a vertically oriented 2D spring element with stiffness k to the elements on the top of the numerical domain, i.e. the top of the embankment. The mpc ensures that the force is interpolated in-between the nodes of the element. Furthermore, after the load is applied and inertia switched back on a velocity that equals the train velocity v_{train} is prescribed to the two nodes of the spring element.

In the current simulations a spring element is generated for each axle, the load is applied without inertia, to prevent vibrations from the initialisation of the load. After this crucial step the train velocity is applied. For each train passage, e.g. one train before and one train after strain accumulation, a set of spring elements need to be generated at the start of the calculation. This is required, as at the end of the simulation of one train passage the spring elements have been moved to the end of the domain.

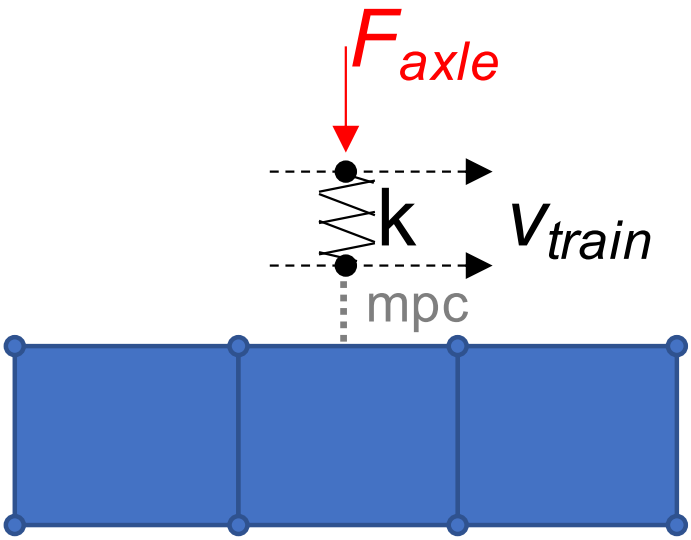

Figure 2.3: *Numerical modelling approach for moving axle loads in FE analysis; The 2D spring elements with stiffnes k transfer the axle load F_{axle} to the main mesh with multipoint constraints mpc; Subsequently the nodes of the spring elements are prescribed with the train velocity v_{train}.*

Finally, this setup allows further refinements in modelling the contact load, e.g. by replacing the axle load F_{axle} with a nodal mass. These masses, however, need to be connected to the other axles in a realistic manner. This, again, can be achieved with special spring (or beam) elements or using multipoint constraints. The proper development for such a moving dynamic load should be considered in future modelling approaches.

2.4 Accumulation parameters from dynamic analysis

The Creep-SClay1Sc cyclic accumulation model is developed starting from experimental data where harmonic loading cycles with a certain period T and loading amplitude q were applied. For numerical problems at boundary value level with non-harmonic loads, it is not trivial to determine appropriate values for T and q for each element in the domain. Whilst the q_{max} is captured for each integration point in the domain with a special option in the constitutive model this cannot be easily replicated for the period T. For q_{max} the current q is simply compared with the highest value recorded until the time step of consideration and only substitutes the value when it is larger. In contrast for T first a series of points at multiple time steps need to be collected for each integration point before the data can be analysed. This requires quite a significant amount of data to be collected and processed, which is not practical as part of the implementation of the constitutive model. In this project some crucial post points are analysed manually for each train velocity and subsequently used for setting the period T in the cyclic accumulation parameters.

2.4.1 Loading period

Fig. 2.4 plots the results of a dynamic analysis of a single moving X2000 passenger carriage. The four axle loads are modelled using the multipoint constraint method. The full modelling details of these analyses will be presented later, however, here the focus is on the mobilisation of the deviatoric stress when the train passes by with two different train velocities, i.e. v_{train} $= 10\,\mathrm{m\,s^{-1}}$ & $v_{train} = 50\,\mathrm{m\,s^{-1}}$. For comparative reasons the time axis that is plotted on the horizontal axis in Fig. 2.4 is multiplied with the train velocity v_{train}. As such the position of the axle loads becomes readily apparent, i.e. 2.9 m between the two axles in a single bogey and 18.3 m between the two bogeys.

The individual axles that lead to an increment in deviatoric load Δq are easily discerned at the top of the embankment, and at the surface of the clay layer albeit with a smaller amplitude. Deeper down in the clay layer, however, this signal is both further attenuated and filtered. The loss of high frequencies with an increased distance from the free surface at the top of the embankment is readily observed in the field, as discussed in (Powrie et al. 2019). In fact, this attribute of Raleigh waves is exploited in some geophysical measurement methods, e.g. (Park et al. 1999).

For the cyclic accumulation model the aim is to arrive at the most reliable time period T as monitored in the soft clay -where the model is used- that (partly) captures the complex loading signal applied at the top of the embankment. The current analyses shows that the bogey – bogey distance L_{bb} and the train velocity v_{train} provide a good estimator for the time period T in the cyclic accumulation model, i.e. Equation 2.2. In further calculations with moving train loads T does not need to be evaluated for each case, rather Equation 2.2 can be used. This greatly simplifies any automated sensitivity analyses and optimisation studies.

$$T = \frac{L_{bb}}{v_{train}} \tag{2.2}$$

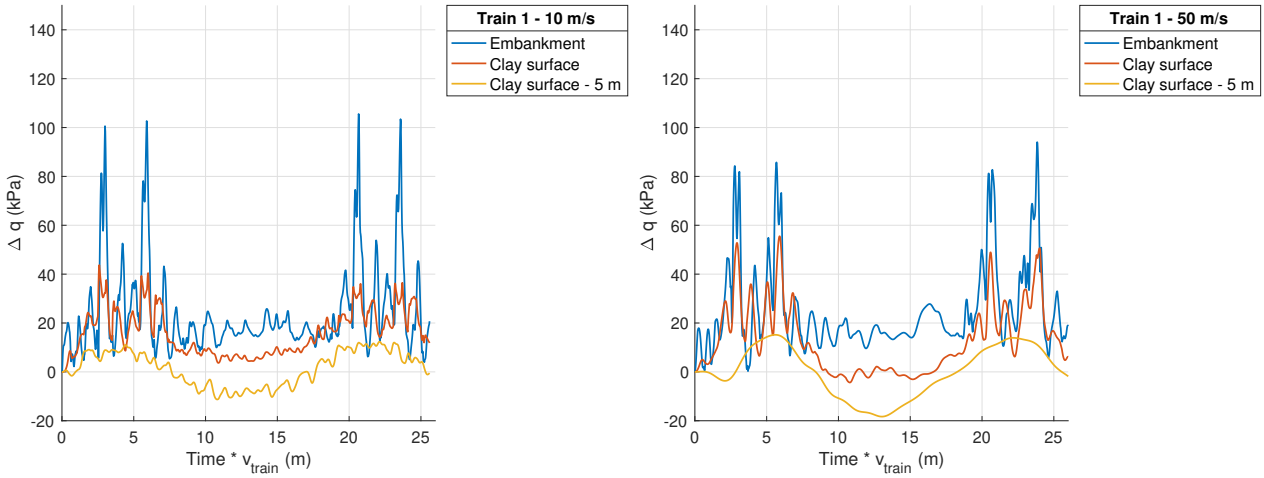

Figure 2.4: *Dynamic response of a moving load of a single carriage with two two-axle bogeys (4 axles total) on an embankment overlaying clay; time axis in distance passing by at observation point;* Δq *is the increment in deviatoric stress. Left:* $v_{train} = 10\,\mathrm{m\,s^{-1}}$*; Right:* $v_{train} = 50\,\mathrm{m\,s^{-1}}$

2.4.2 Deviatoric loading amplitude

The maximum deviatoric loading amplitude Δq_{max} is recorded by the Creep-Sclay1Sc model during the simulation of a single train passage. Given only the loading amplitude is of interest both the minimum and maximum stress level are tracked. Fig. 2.5left shows the recorded Δq_{max} for several horizontal cross sections as function of depth. The horizontal axis plots the width of modelled clay layer which is 50 m. Similarly Fig. 2.5right shows Δq_{max} for several vertical cross sections. The modelled clay layer is 40 m. It is not as easy to capture Δq_{max} in parts of the domain that are modelled with the standard models of the FE code.

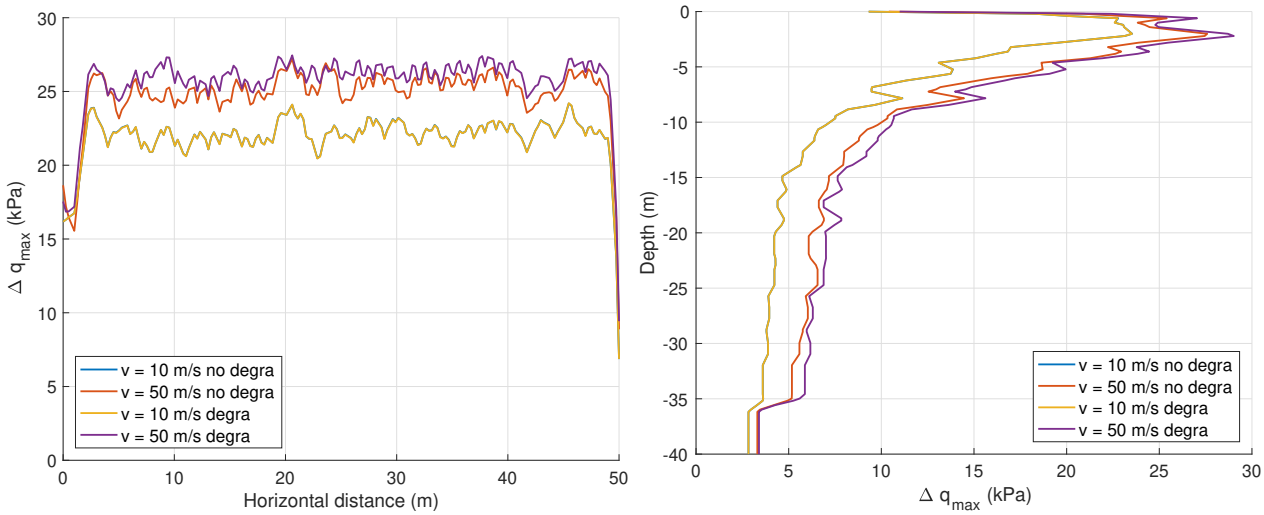

Figure 2.5: Δq_{max} *for a horizontal cross section just below the surface of the clay layer (left) and a vertical cross-section halfway at* $x = 25\,\mathrm{m}$ *(right). Results are shown for the cyclic accumulation model with (degra) and without stiffness degradation (no degra) and two train velocities.*

The results indicate that a moving train load leads to a uniform maximum deviatoric stress as function of horizontal distance which attenuates reasonably quickly with depth. This further supports the use of a quasi-static cyclic accumulation model with a uniform loading period and amplitude as input parameter and state variable. Furthermore, the effect of stiffness degradation during the first loading sequence (before cyclic accumulation) seems to be more pronounced for larger train velocities (that generate larger inertial loads).

In subsequent trial calculations the constitutive model, as implemented right now, proves to be numerically unstable for these large magnitudes Δq_{max}. At the writing of this report it is postulated that this is partly due to the model parameters chosen for the boundary value analyses and partly due to the model implementation. A mean value of $\Delta q_{max} = 10\,\text{kPa}$ that is more uniform as function of depth has been used instead in order to capture the main effects without issues with convergence.

2.5 Numerical model for transition zone

2.5.1 Geometry & mesh

The numerical model is shown in Fig. 2.6. A 2D plane strain longitudinal section of 100 m wide and 41 m height is generated. The embankment of 1 m height is overlaying a 50 m wide soft clay layer of 40 m height on the left and a stiff soil on the right with similar dimensions. The water table is at the surface of the clay layer (subgrade) directly below the embankment. For each wheel a spring element and multipoint contraint is generated. Two sets of 4 wheels are generated in order to model two train passages in one calculation, i.e. one passage prior and one passage after the cyclic accumulation stage of the simulations. The side boundaries are fixed for horizontal displacements and impermeable, whereas the lower boundary fixes the vertical displacements and is also impermeable. The use of damping boundaries has been avoided.

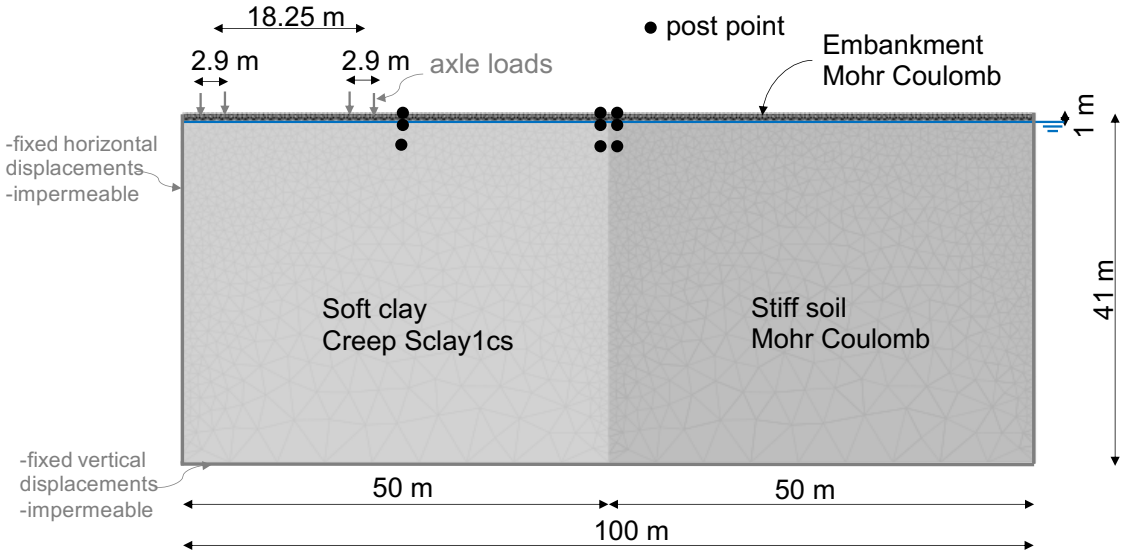

Figure 2.6: *Numerical model for transition zone with triangular mesh, boundary conditions, constitutive model and post points annotated.*

2.5.2 Constitutive models

The soft clay is modelled with the Creep-Sclay1Sc cyclic accumulation model, both the original version and the modified version with stiffness degradation are used. See Tables 2.1 & 2.2 for an overview of the model parameters of respectively the base Creep-Sclay1S model . The embankment and stiff soil both are modelled using a Mohr Coulomb elasto-plastic model of which the properties are listed in Table 2.3. The stiffness in both models, i.e. κ and E' have been increased by a factor 5 to better reflect the stiff response under small strain loading. The stiffness in the spring elements is chosen to be large compared to the stiffness of the soil, i.e. $k = 1.0 \times 10^7$ kPa. The horizontal and vertical hydraulic conductivities k_hc & k_vc are both set at $1.0 \times 10^{-8}\,\mathrm{m\,s^{-1}}$ in the clay, k_he & k_ve are $1.0 \times 10^{-1}\,\mathrm{m\,s^{-1}}$ in the embankment and k_hss & k_vss are $1.0 \times 10^{-2}\,\mathrm{m\,s^{-1}}$ in the stiff sand layer. The storage modulus C in the groundwater flow equations is set at $1.0 \times 10^{-7}\,\mathrm{kPa^{-1}}$.

Table 2.1: Model parameters for Creep-SClay1Sc in the soft soil (Onsøy clay).

Parameter	Definition	Unit	Value
λ_i^*	Modified intrinsic compression index	[-]	0.076
κ^*	Modified swelling index	[-]	0.002
ν	Poisson's ratio	[-]	0.15
M_c	Stress ratio at critical state in triaxial compression	[-]	1.23
M_e	Stress ratio at critical state in triaxial extension	[-]	0.8
ω	Rate of rotation	[-]	200
ω_d	Rate of rotation due to deviator strain rate	[-]	0.56
a	Rate of destructuration	[-]	10
b	Rate of destructuration due to deviator strain rate	[-]	0.30
POP	Pre overburden pressure	[kPa]	20
e_0	Initial void ratio	[-]	1.8
α_0	Initial anisotropy	[-]	0.47
χ_0	Initial amount of bonding	[-]	10
μ_i^*	Modified intrinsic creep index	[-]	0.005
τ	Reference time	[day]	1

Table 2.2: Cyclic parameters for Creep-SClay1Sc (Onsøy clay).

Parameter	Definition	Unit	Value
ζ	Axial strain accumulation factor in undrained cyclic triaxial test	[day]	1.17×10^{-3}
ι	Effectiveness of cyclic deviator stress	[-]	1.81×10^{-4}
Ξ	Loading period dependency	[-]	$seetext$
Γ_{alpha}	Scaling factor to set cyclic reference time	[-]	2.91×10^{-5}
Γ_{beta}	Scaling factor to set cyclic reference time	[-]	5.92
r	Stiffness reduction factor	[-]	0.8

2.5.3 Case study

The transition zone shown in Fig. 2.6 is studied for a total of four cases. The construction of the embankment and its associated change in soil properties below are not explicitly modelled. Rather a pre-overburden pressure that is close the self weight of the embankment has been used.

Table 2.3: Elasto-plastic parameters for the embankment and stiff soil.

Material	Parameter	units	value
Embankment	Young's modulus	[kPa]	1.0×10^5
	Poisson's ratio	[-]	0.3
	Friction angle	[°]	35
	Dilatancy angle	[°]	0
	Cohesion	[kPa]	10
Stiff soil	Young's modulus	[kPa]	1.0×10^5
	Poisson's ratio	[-]	0.3
	Friction angle	[°]	35
	Dilatancy angle	[°]	0
	Cohesion	[kPa]	0

Hence, settlements from consolidation or creep will be benign. The case studies considered vary two aspects of the simulation. The first aspect focuses on the effect of the train velocity. One very slow train with $v_{train} = 10\,\mathrm{m\,s^{-1}}$ and a fast train $v_{train} = 50\,\mathrm{m\,s^{-1}}$ are simulated, which also required changing Ξ to reflect the loading period T in the model. In both cases the axle spacings of a X2000 passenger carriage with a load of $F_{axle} = 60\,\mathrm{kN}$ are used. These simulations are repeated for the model with stiffness degradation, that allows up to 20% reduction of κ as function of the destructuration parameter χ. Find the full overview in Table 2.4

Table 2.4: Cases studied.

Case #	Model version	Train velocity	Unit
1	No degradation	10	$[\mathrm{m\,s^{-1}}]$
2	No degradation	50	$[\mathrm{m\,s^{-1}}]$
3	With degradation	10	$[\mathrm{m\,s^{-1}}]$
4	With degradation	50	$[\mathrm{m\,s^{-1}}]$

3 Results

3.1 Introduction

The cyclic strain accumulation model is used to investigate the effect of train velocity v_{train} and and model type on the change in dynamic response for a 4 axle train passing by. In between two train passages, i.e. train 1 & train 2, the cyclic accumulation model simulates 100 000 loading cycles using the amplitude q_{tmax} and period T as described in the previous chapter. The results for the change in effective stress during a train passage are decomposed in mean effective stress $\Delta p'$ (isotropic) and deviatoric stress Δq (shear), additionally the change in pore water pressures Δu and the vertical accelerations a that are normalised with the gravitational accelerations g $= 9.81\,\mathrm{m\,s^{-2}}$ are also shown. Each plot represents a horizontal position in space, i.e. halfway the clay domain $x = 25\,\mathrm{m}$, one meter before the transition $x = 49\,\mathrm{m}$ and one meter after the transition $x = 51\,\mathrm{m}$. In each section three data series are shown, one for each depth: top of the embankment $z = 41\,\mathrm{m}$, the surface of the clay layer directly below the embankment at $z =$ $40\,\mathrm{m}$ and a point in the clay at $z = 35\,\mathrm{m}$. The sign convention follows structural mechanics, e.g. a negative value for $\Delta p'$ equates to a compressive stress. Furthermore, a positive acceleration is pointed upwards, whereas a negative magnitude for acceleration is downwards. For ease of comparison between the different scenarios the horizontal axis shows the simulation time multiplied by the train velocity v_{train}.

3.2 Increase in deviatoric stress Δq

3.2.1 $x = 25\,\mathrm{m}$

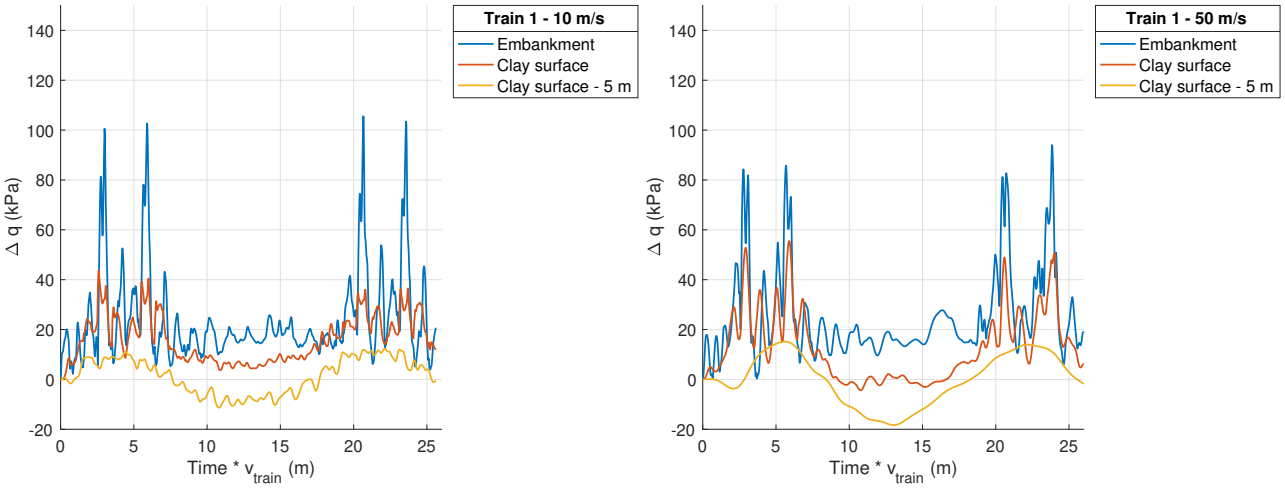

(a) *Train 1:* $v_{train} = 10\,\mathrm{m\,s^{-1}}$.

(b) *Train 1:* $v_{train} = 50\,\mathrm{m\,s^{-1}}$.

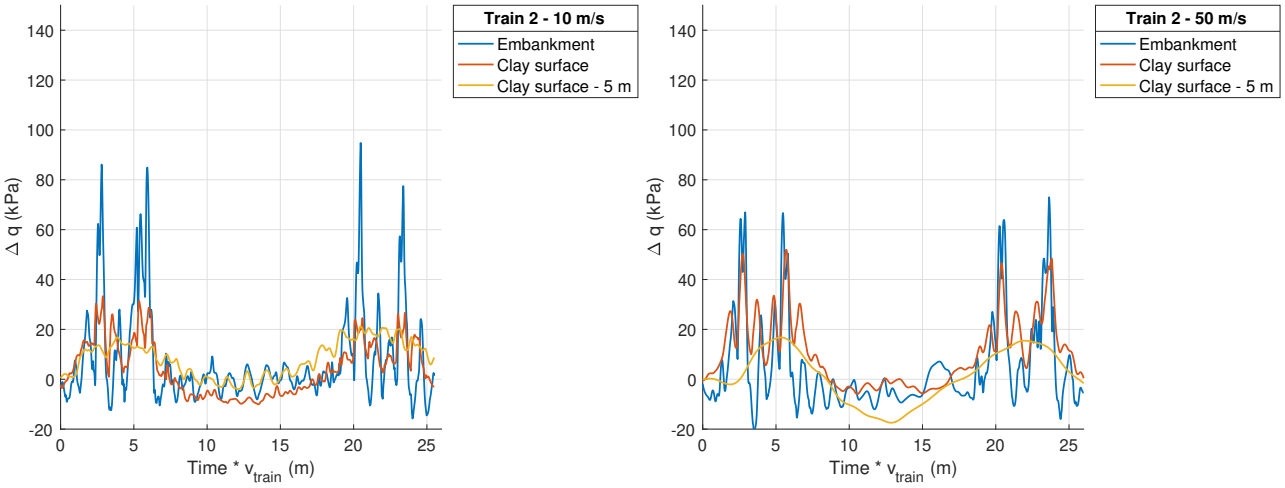

(c) *Train 2:* $v_{train} = 10\,\mathrm{m\,s^{-1}}$.

(d) *Train 2:* $v_{train} = 50\,\mathrm{m\,s^{-1}}$.

Figure 3.1: Δq *for train 1 (before cycle 1) & train 2 (after cycle 100k);* $x = 25\,\mathrm{m}$*; no stiffness degradation in model.*

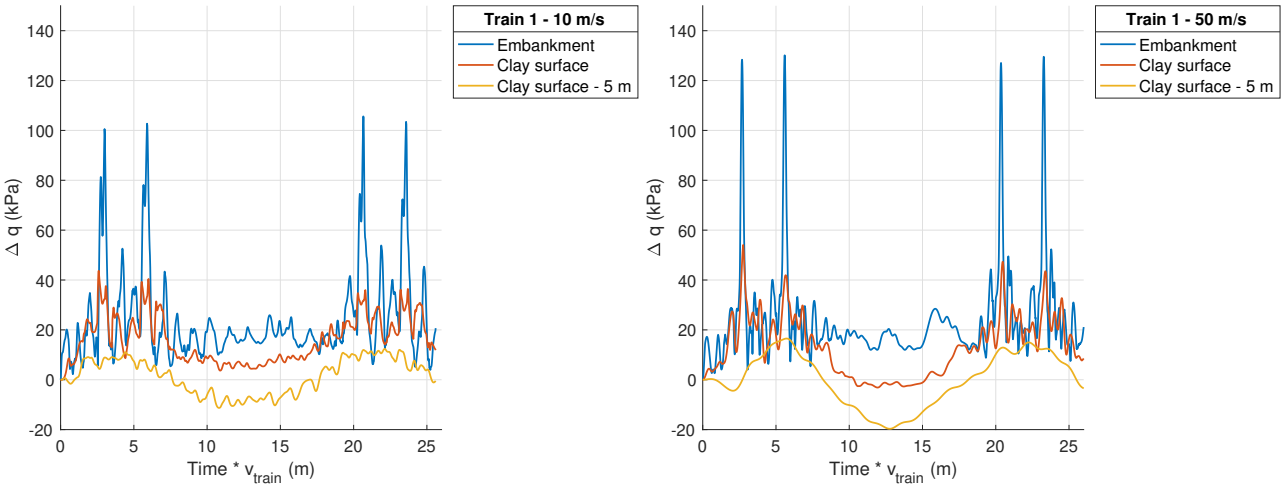

(a) *Train 1:* $v_{train} = 10\,\mathrm{m\,s^{-1}}$.

(b) *Train 1:* $v_{train} = 50\,\mathrm{m\,s^{-1}}$.

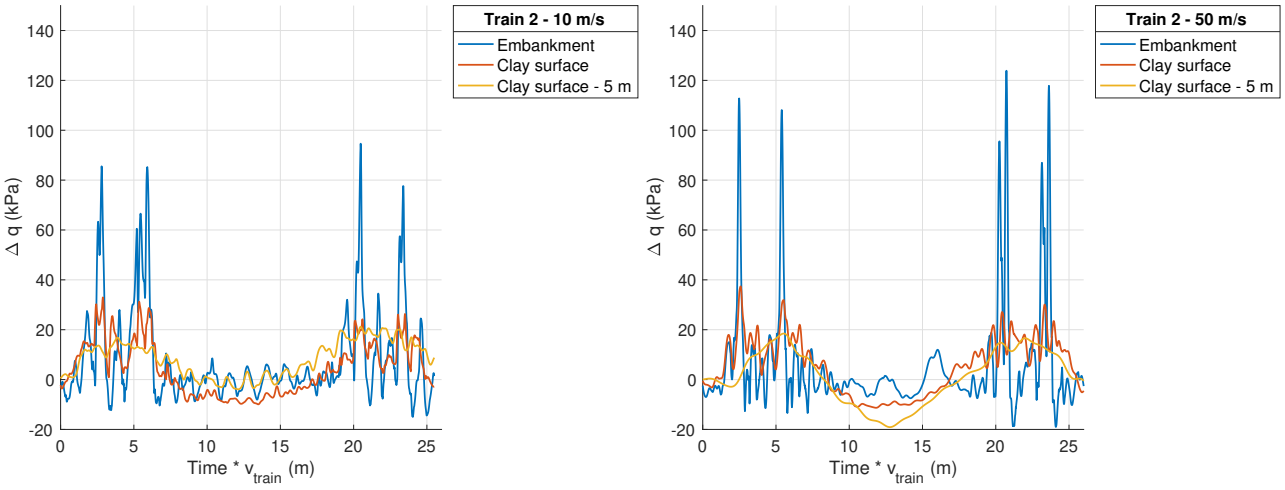

(c) *Train 2:* $v_{train} = 10\,\mathrm{m\,s^{-1}}$.

(d) *Train 2:* $v_{train} = 50\,\mathrm{m\,s^{-1}}$.

Figure 3.2: Δq *for train 1 (before cycle 1) & train 2 (after cycle 100k);* $x = 25\,\mathrm{m}$*; with stiffness degradation in model.*

3.2.2 $x = 49\,\mathrm{m}$

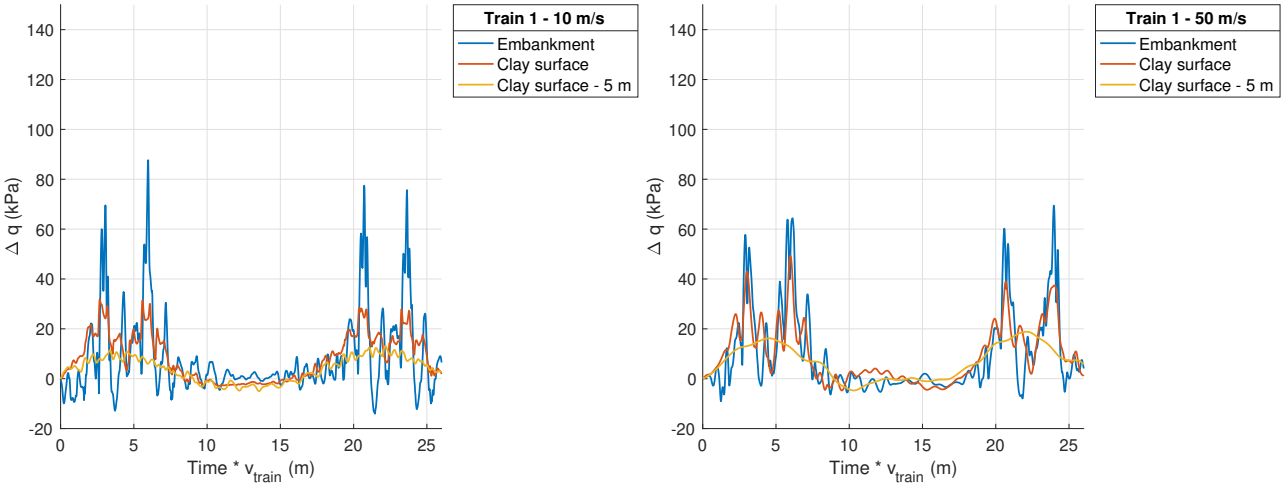

(a) *Train 1:* $v_{train} = 10\,\mathrm{m\,s^{-1}}$.

(b) *Train 1:* $v_{train} = 50\,\mathrm{m\,s^{-1}}$.

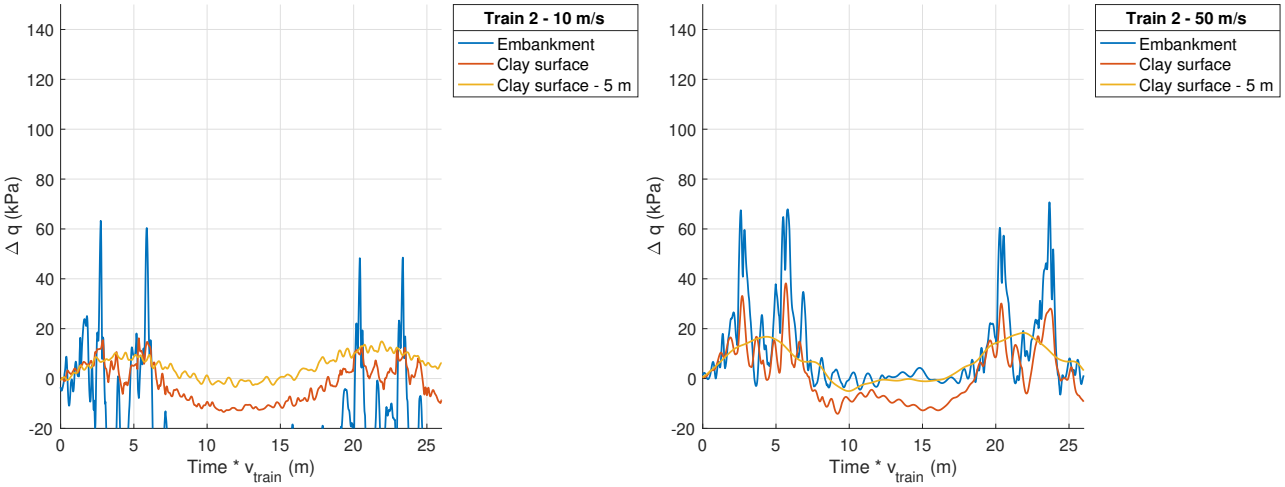

(c) *Train 2:* $v_{train} = 10\,\mathrm{m\,s^{-1}}$.

(d) *Train 2:* $v_{train} = 50\,\mathrm{m\,s^{-1}}$.

Figure 3.3: Δq *for train 1 (before cycle 1) & train 2 (after cycle 100k);* $x = 25\,\mathrm{m}$*; no stiffness degradation in model.*

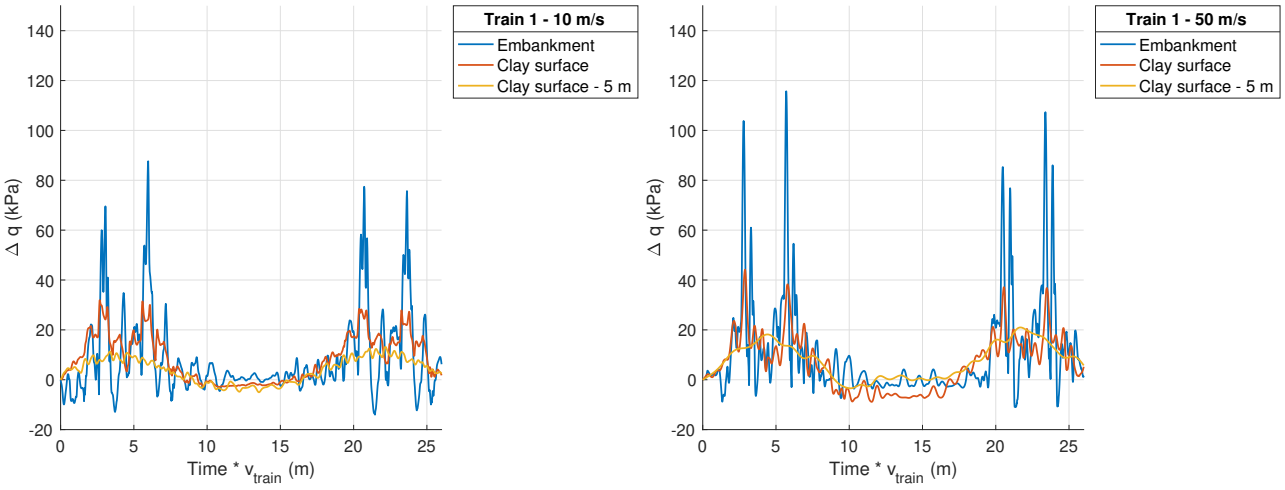

(a) *Train 1:* $v_{train} = 10\,\mathrm{m\,s^{-1}}$.

(b) *Train 1:* $v_{train} = 50\,\mathrm{m\,s^{-1}}$.

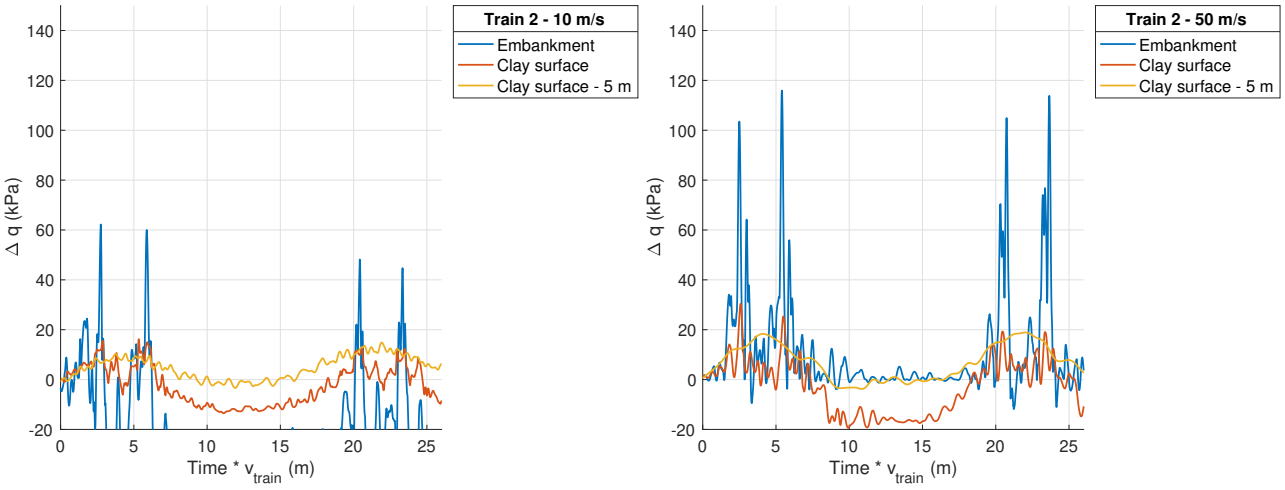

(c) *Train 2:* $v_{train} = 10\,\mathrm{m\,s^{-1}}$.

(d) *Train 2:* $v_{train} = 50\,\mathrm{m\,s^{-1}}$.

Figure 3.4: Δq *for train 1 (before cycle 1) & train 2 (after cycle 100k);* $x = 49\,\mathrm{m}$*; with stiffness degradation in model.*

3.2.3 $x = 51\,\mathrm{m}$

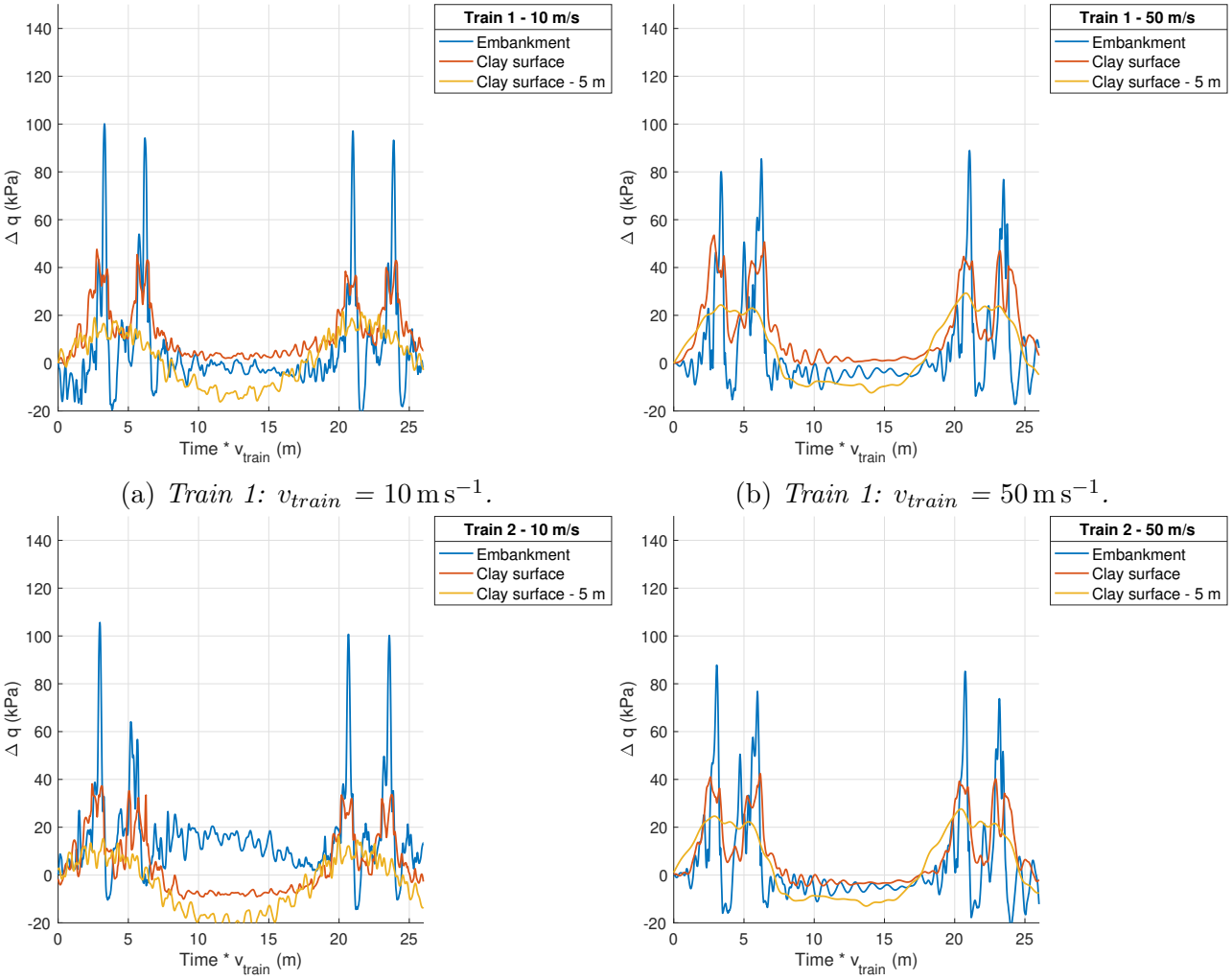

(a) *Train 1:* $v_{train} = 10\,\mathrm{m\,s^{-1}}$.

(b) *Train 1:* $v_{train} = 50\,\mathrm{m\,s^{-1}}$.

(c) *Train 2:* $v_{train} = 10\,\mathrm{m\,s^{-1}}$.

(d) *Train 2:* $v_{train} = 50\,\mathrm{m\,s^{-1}}$.

Figure 3.5: Δq *for train 1 (before cycle 1) & train 2 (after cycle 100k);* $x = 51\,\mathrm{m}$*; no stiffness degradation in model.*

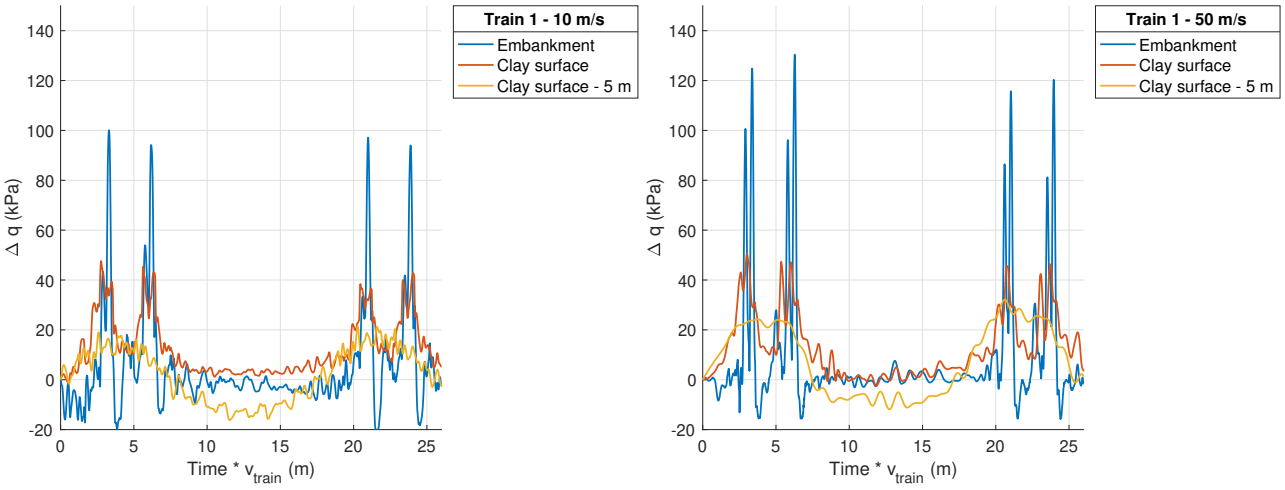

(a) *Train 1:* $v_{train} = 10\,\mathrm{m\,s^{-1}}$.

(b) *Train 1:* $v_{train} = 50\,\mathrm{m\,s^{-1}}$.

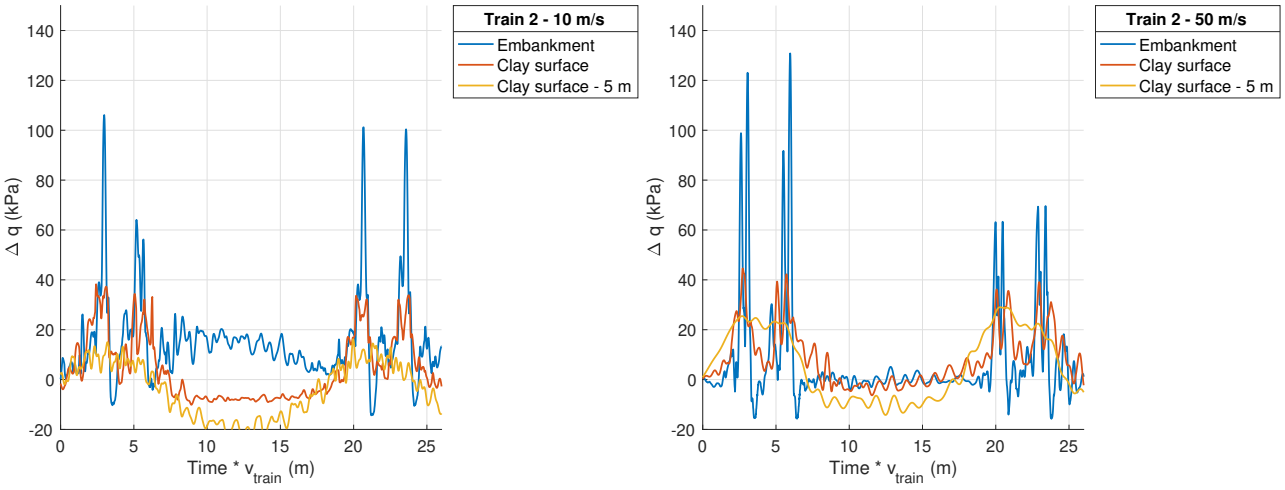

(c) *Train 2:* $v_{train} = 10\,\mathrm{m\,s^{-1}}$.

(d) *Train 2:* $v_{train} = 50\,\mathrm{m\,s^{-1}}$.

Figure 3.6: Δq *for train 1 (before cycle 1) & train 2 (after cycle 100k);* $x = 51\,\mathrm{m}$*; with stiffness degradation in model.*

3.3 Increase in mean effective stress $\Delta p'$

3.3.1 $x = 25\,\mathrm{m}$

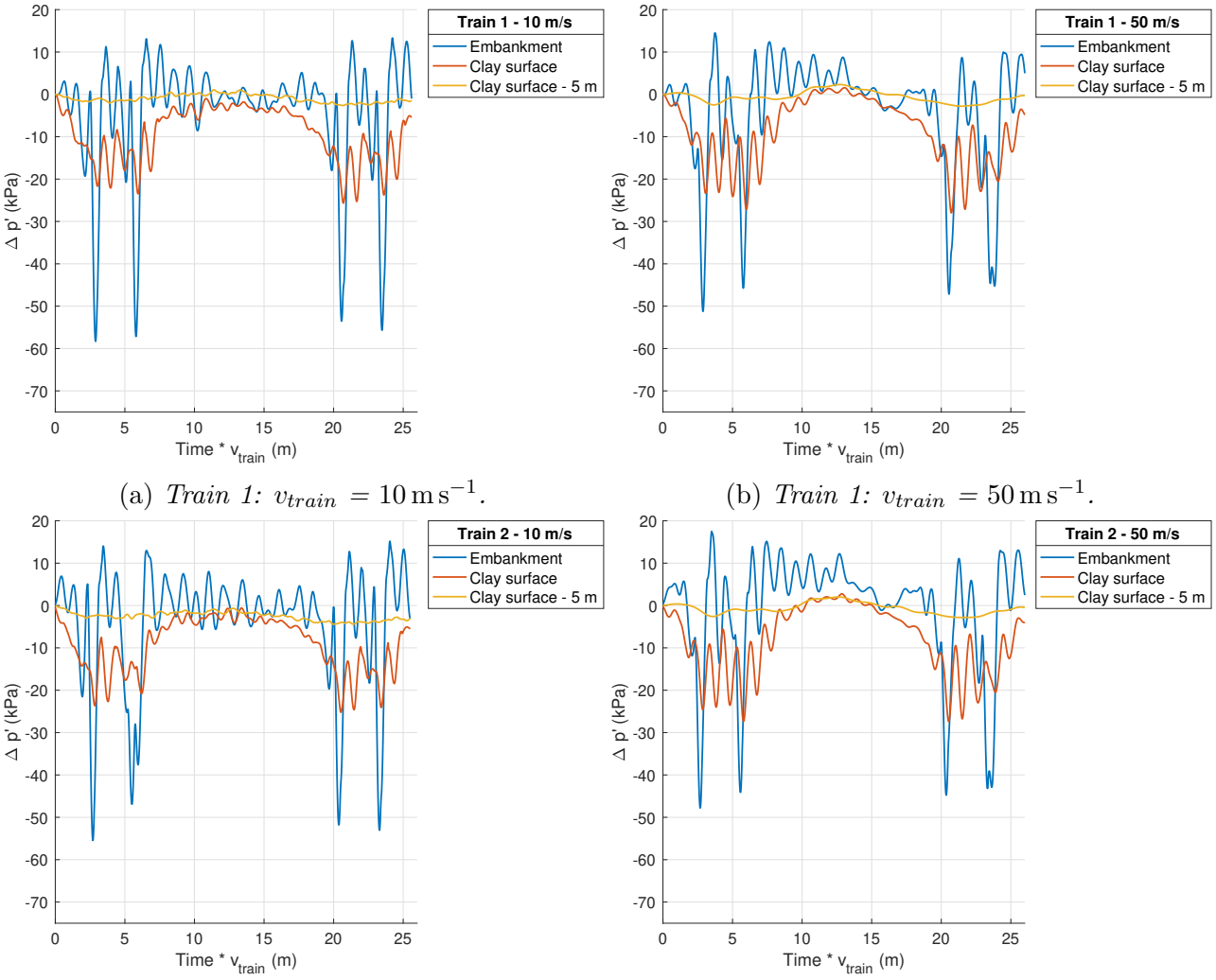

(a) *Train 1:* $v_{train} = 10\,\mathrm{m\,s^{-1}}$.

(b) *Train 1:* $v_{train} = 50\,\mathrm{m\,s^{-1}}$.

(c) *Train 2:* $v_{train} = 10\,\mathrm{m\,s^{-1}}$.

(d) *Train 2:* $v_{train} = 50\,\mathrm{m\,s^{-1}}$.

Figure 3.7: $\Delta p'$ *for train 1 (before cycle 1) & train 2 (after cycle 100k);* $x = 25\,\mathrm{m}$*; no stiffness degradation in model.*

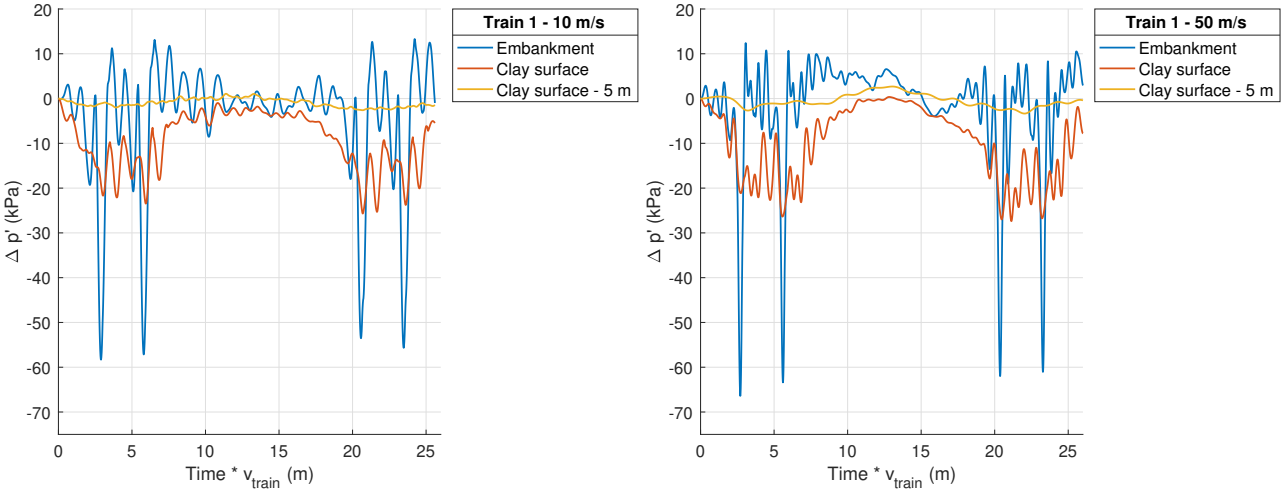

(a) *Train 1:* $v_{train} = 10\,\mathrm{m\,s^{-1}}$.

(b) *Train 1:* $v_{train} = 50\,\mathrm{m\,s^{-1}}$.

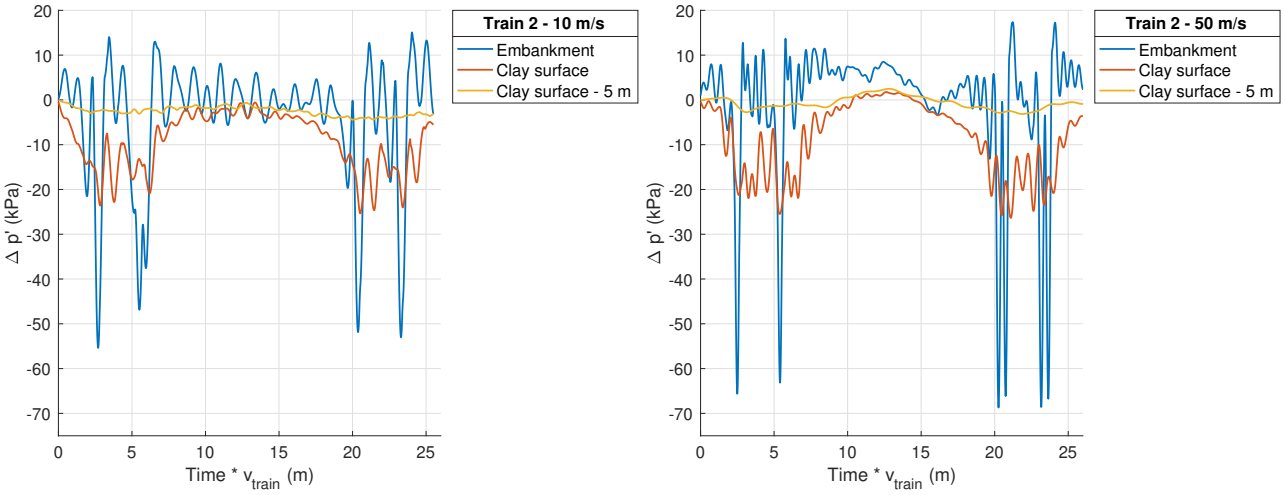

(c) *Train 2:* $v_{train} = 10\,\mathrm{m\,s^{-1}}$.

(d) *Train 2:* $v_{train} = 50\,\mathrm{m\,s^{-1}}$.

Figure 3.8: $\Delta p'$ *for train 1 (before cycle 1) & train 2 (after cycle 100k);* $x = 25\,\mathrm{m}$*; with stiffness degradation in model.*

3.3.2 $x = 49\,\mathrm{m}$

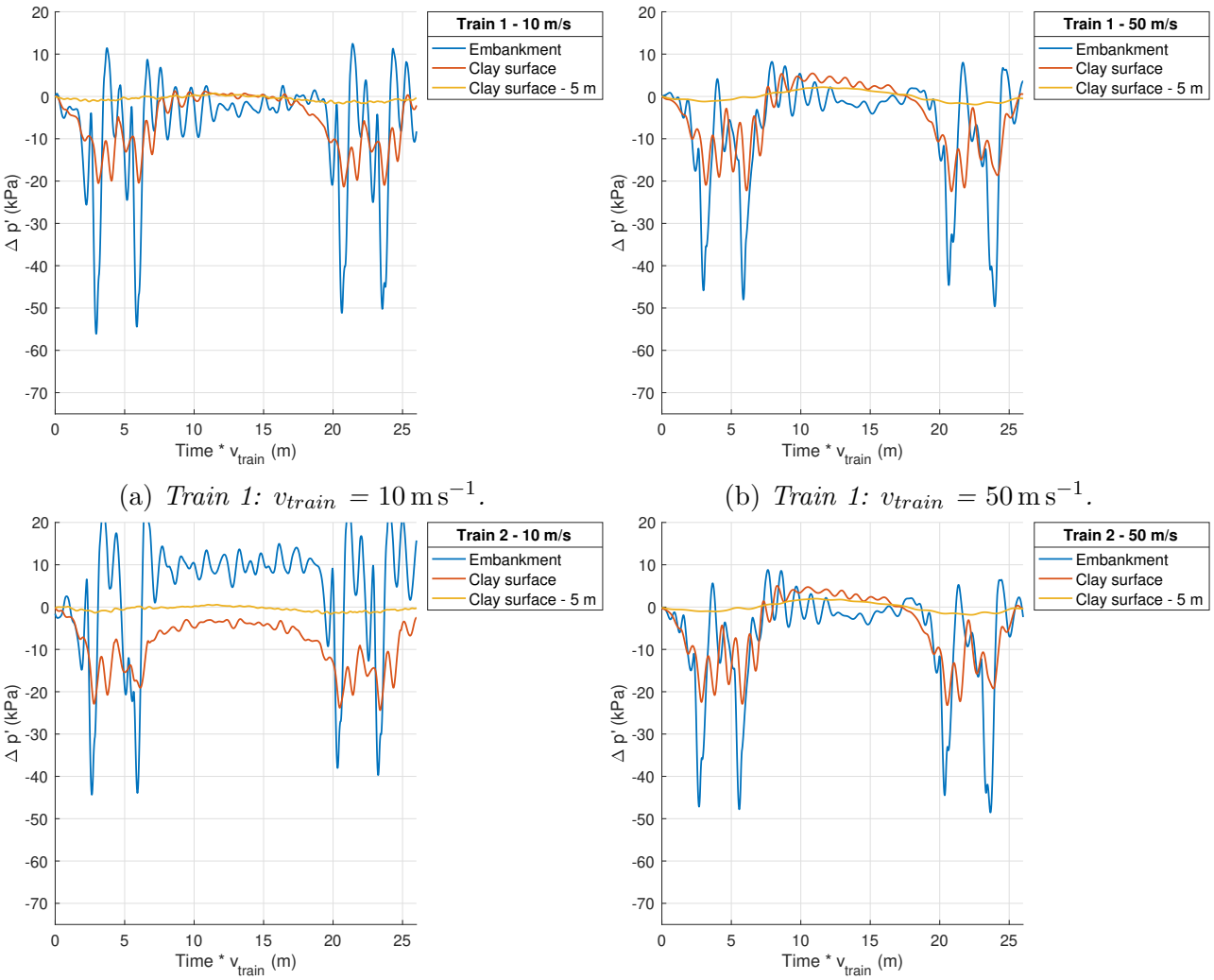

(a) *Train 1:* $v_{train} = 10\,\mathrm{m\,s^{-1}}$.

(b) *Train 1:* $v_{train} = 50\,\mathrm{m\,s^{-1}}$.

(c) *Train 2:* $v_{train} = 10\,\mathrm{m\,s^{-1}}$.

(d) *Train 2:* $v_{train} = 50\,\mathrm{m\,s^{-1}}$.

Figure 3.9: $\Delta p'$ *for train 1 (before cycle 1) & train 2 (after cycle 100k);* $x = 25\,\mathrm{m}$*; no stiffness degradation in model.*

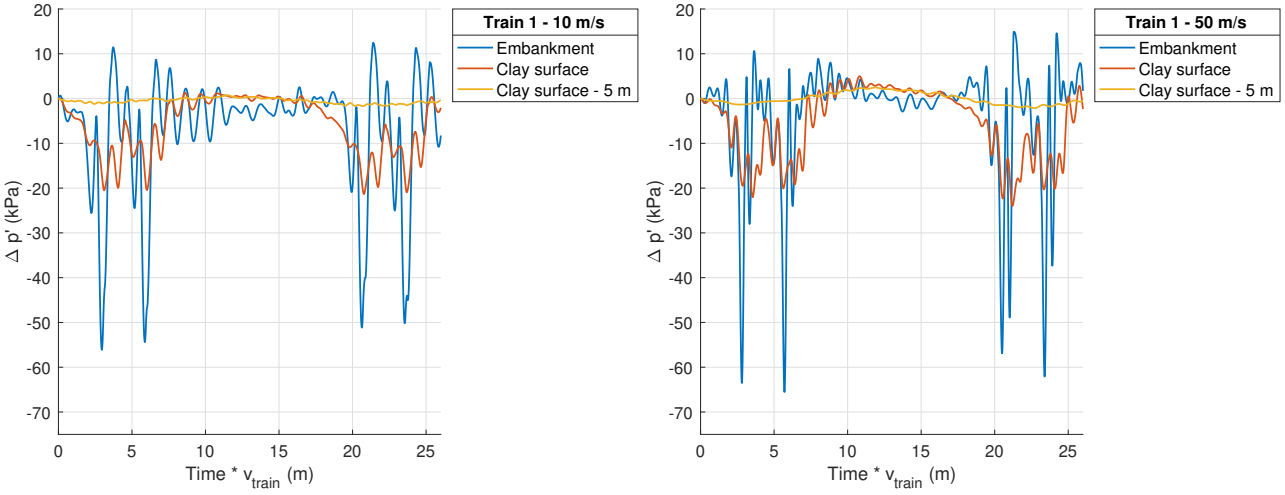

(a) *Train 1:* $v_{train} = 10\,\mathrm{m\,s^{-1}}$.

(b) *Train 1:* $v_{train} = 50\,\mathrm{m\,s^{-1}}$.

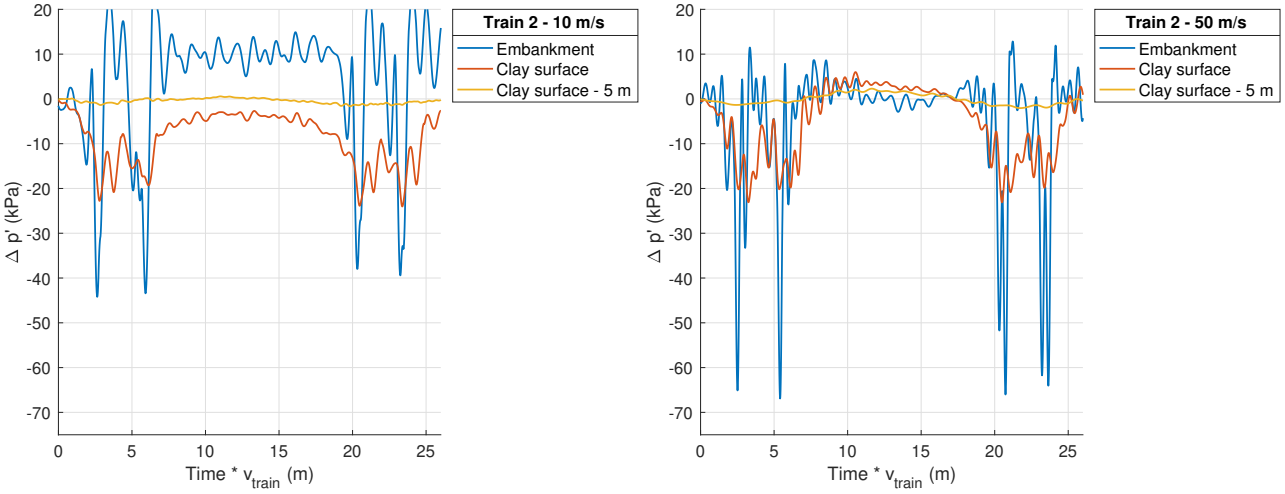

(c) *Train 2:* $v_{train} = 10\,\mathrm{m\,s^{-1}}$.

(d) *Train 2:* $v_{train} = 50\,\mathrm{m\,s^{-1}}$.

Figure 3.10: $\Delta p'$ *for train 1 (before cycle 1) & train 2 (after cycle 100k);* $x = 49\,\mathrm{m}$*; with stiffness degradation in model.*

3.3.3 $x = 51\,\mathrm{m}$

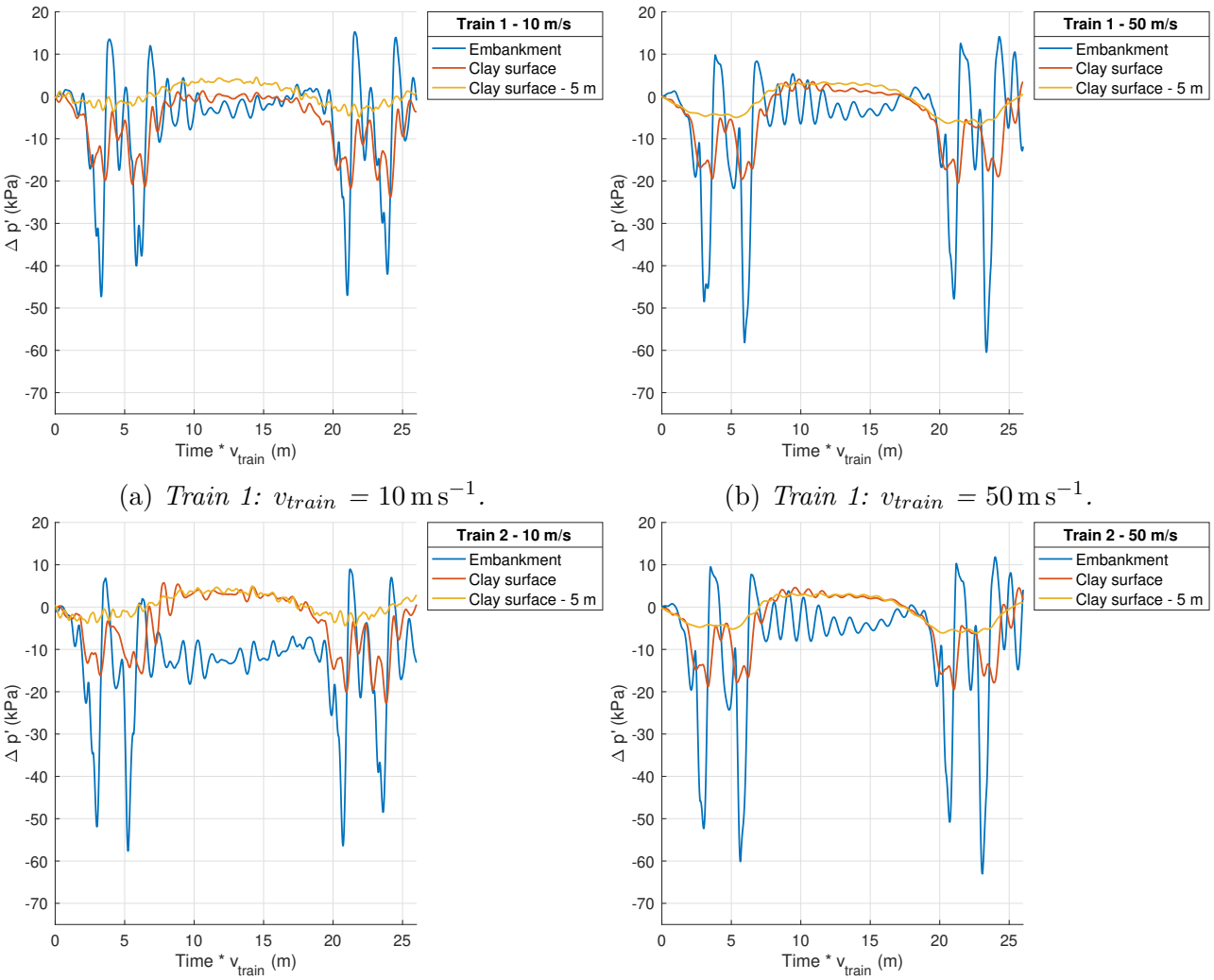

(a) *Train 1:* $v_{train} = 10\,\mathrm{m\,s^{-1}}$.

(b) *Train 1:* $v_{train} = 50\,\mathrm{m\,s^{-1}}$.

(c) *Train 2:* $v_{train} = 10\,\mathrm{m\,s^{-1}}$.

(d) *Train 2:* $v_{train} = 50\,\mathrm{m\,s^{-1}}$.

Figure 3.11: Δq *for train 1 (before cycle 1) & train 2 (after cycle 100k);* $x = 51\,\mathrm{m}$*; no stiffness degradation in model.*

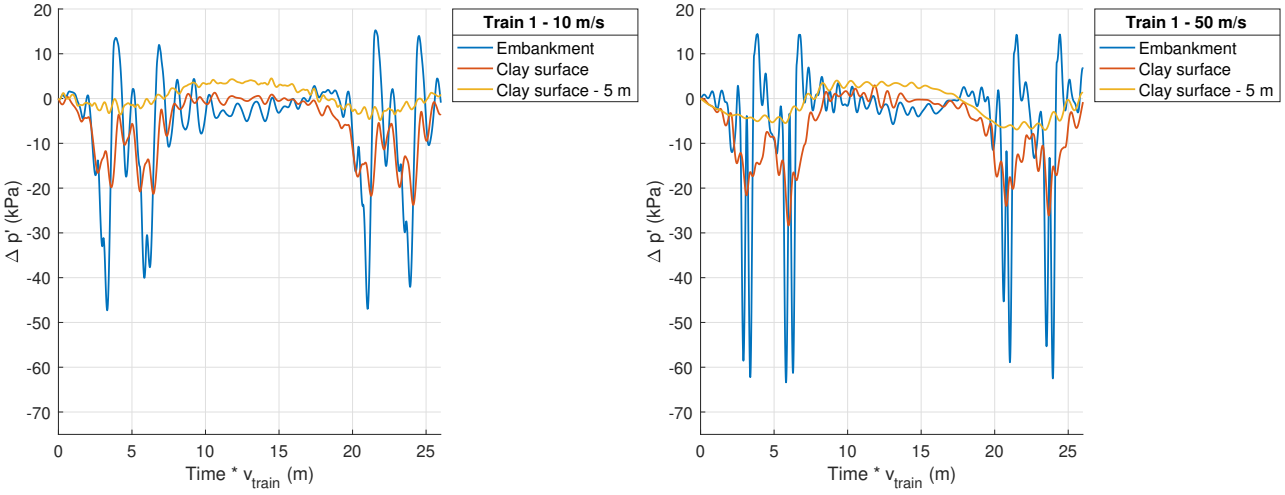

(a) *Train 1:* $v_{train} = 10\,\mathrm{m\,s^{-1}}$.

(b) *Train 1:* $v_{train} = 50\,\mathrm{m\,s^{-1}}$.

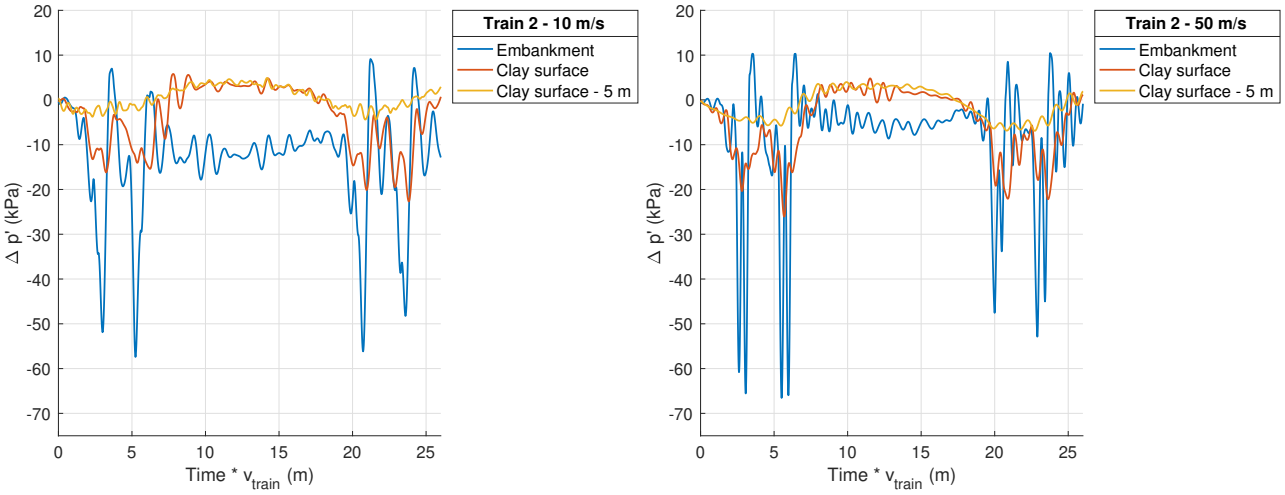

(c) *Train 2:* $v_{train} = 10\,\mathrm{m\,s^{-1}}$.

(d) *Train 2:* $v_{train} = 50\,\mathrm{m\,s^{-1}}$.

Figure 3.12: $\Delta p'$ *for train 1 (before cycle 1) & train 2 (after cycle 100k);* $x = 51\,\mathrm{m}$*; with stiffness degradation in model.*

3.4 Generation of excess pore water pressure Δu

3.4.1 $x = 25\,\mathrm{m}$

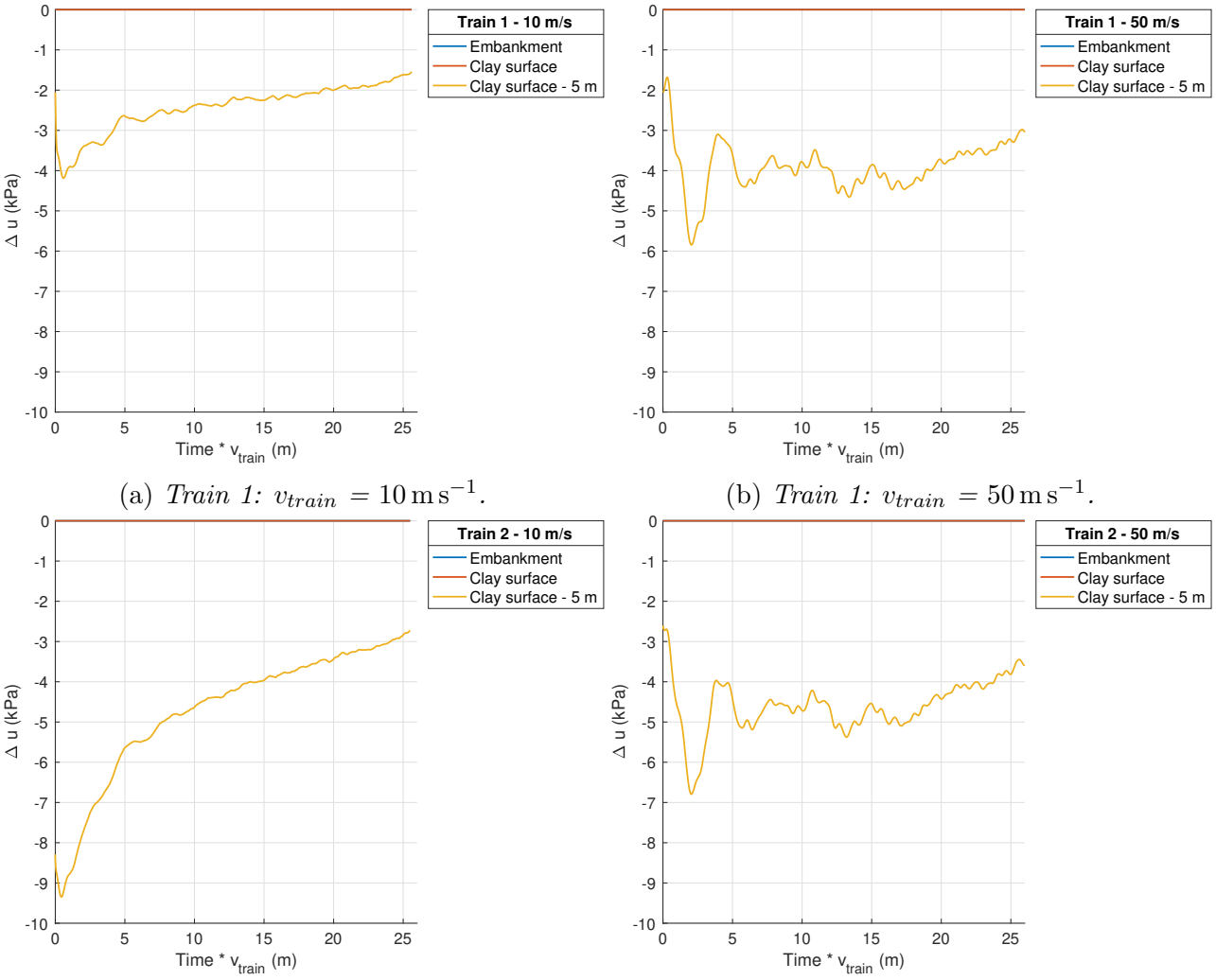

(a) *Train 1:* $v_{train} = 10\,\mathrm{m\,s^{-1}}$.

(b) *Train 1:* $v_{train} = 50\,\mathrm{m\,s^{-1}}$.

(c) *Train 2:* $v_{train} = 10\,\mathrm{m\,s^{-1}}$.

(d) *Train 2:* $v_{train} = 50\,\mathrm{m\,s^{-1}}$.

Figure 3.13: Δu *for train 1 (before cycle 1) & train 2 (after cycle 100k);* $x = 25\,\mathrm{m}$*; no stiffness degradation in model.*

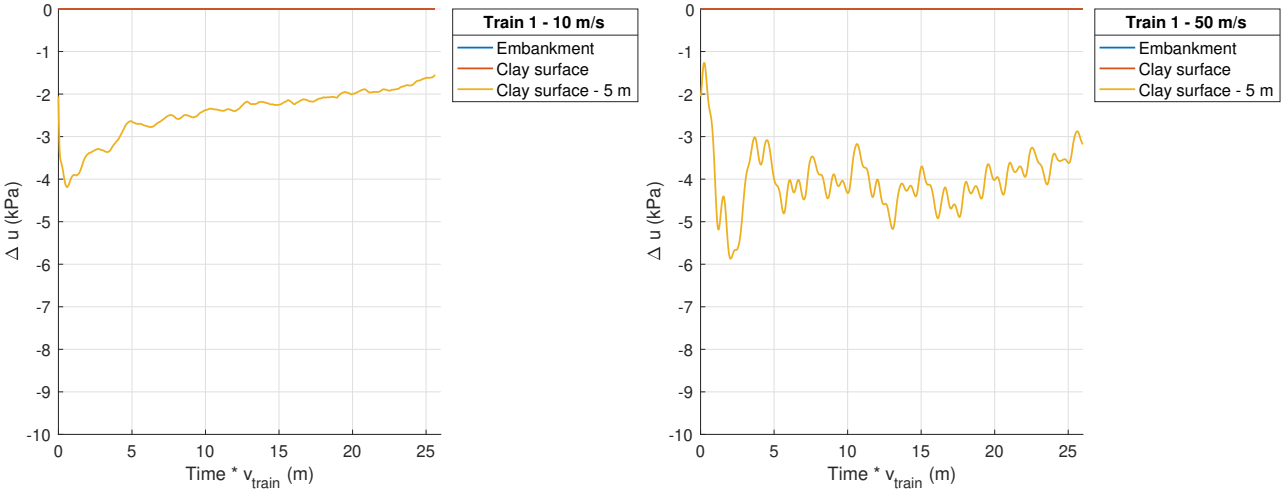

(a) *Train 1:* $v_{train} = 10\,\mathrm{m\,s^{-1}}$.

(b) *Train 1:* $v_{train} = 50\,\mathrm{m\,s^{-1}}$.

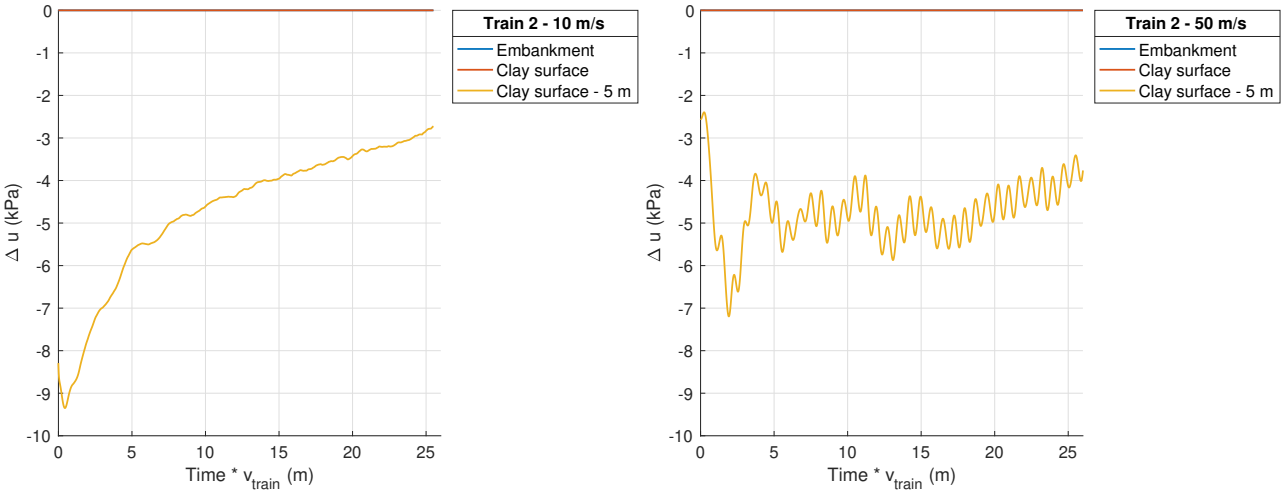

(c) *Train 2:* $v_{train} = 10\,\mathrm{m\,s^{-1}}$.

(d) *Train 2:* $v_{train} = 50\,\mathrm{m\,s^{-1}}$.

Figure 3.14: Δu *for train 1 (before cycle 1) & train 2 (after cycle 100k);* $x = 25\,\mathrm{m}$*; with stiffness degradation in model.*

3.4.2 $x = 49\,\mathrm{m}$

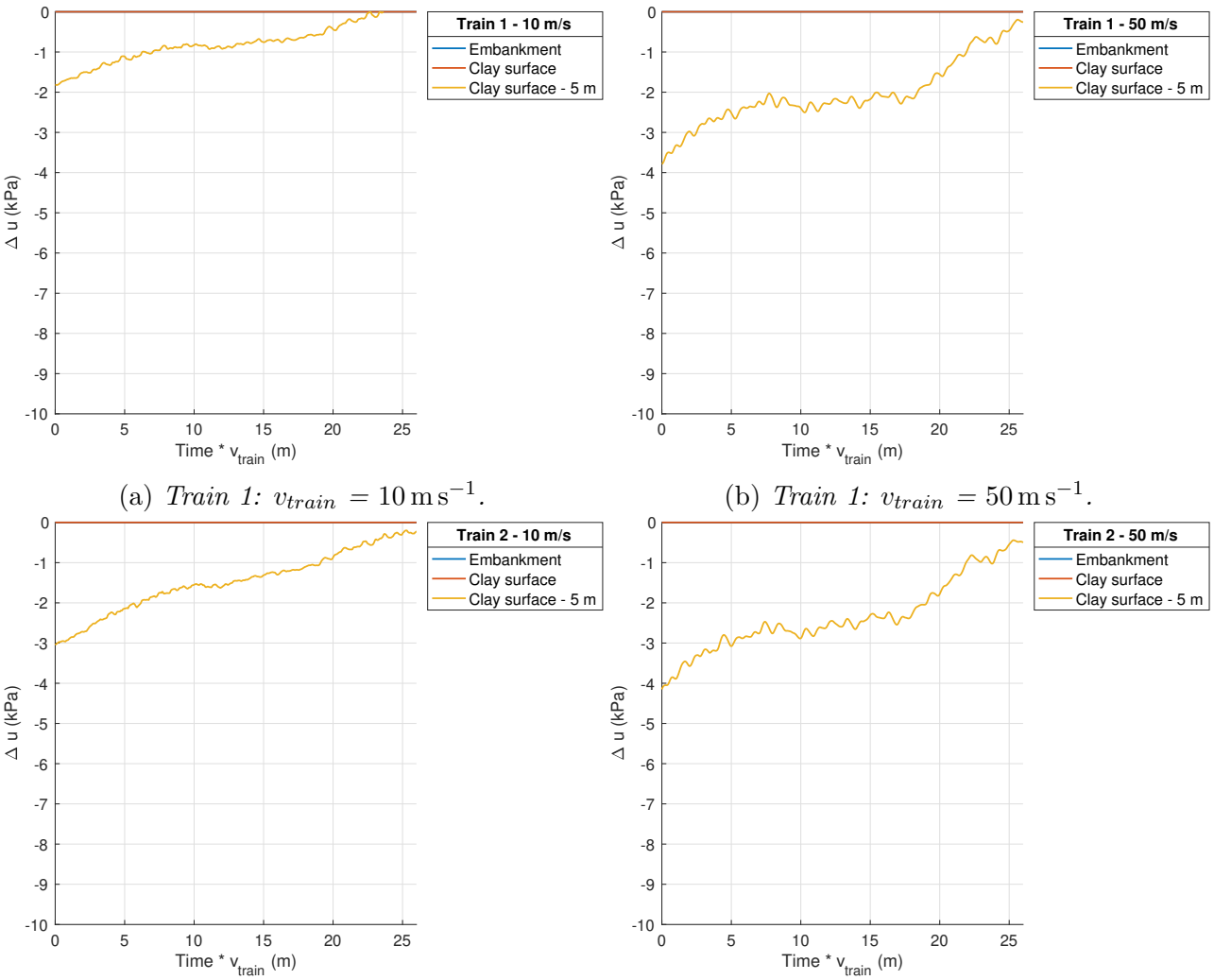

(a) *Train 1:* $v_{train} = 10\,\mathrm{m\,s^{-1}}$.

(b) *Train 1:* $v_{train} = 50\,\mathrm{m\,s^{-1}}$.

(c) *Train 2:* $v_{train} = 10\,\mathrm{m\,s^{-1}}$.

(d) *Train 2:* $v_{train} = 50\,\mathrm{m\,s^{-1}}$.

Figure 3.15: Δu *for train 1 (before cycle 1) & train 2 (after cycle 100k);* $x = 25\,\mathrm{m}$*; no stiffness degradation in model.*

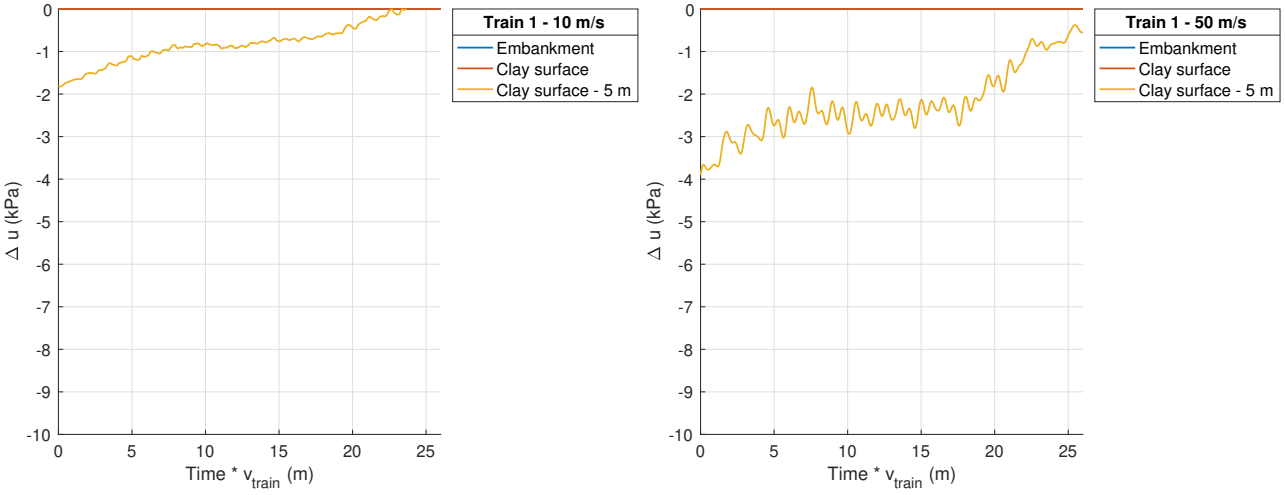

(a) *Train 1:* $v_{train} = 10\,\mathrm{m\,s^{-1}}$.

(b) *Train 1:* $v_{train} = 50\,\mathrm{m\,s^{-1}}$.

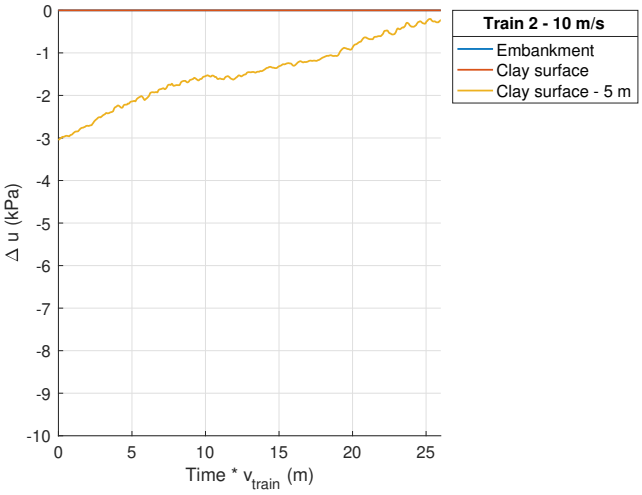

(c) *Train 2:* $v_{train} = 10\,\mathrm{m\,s^{-1}}$.

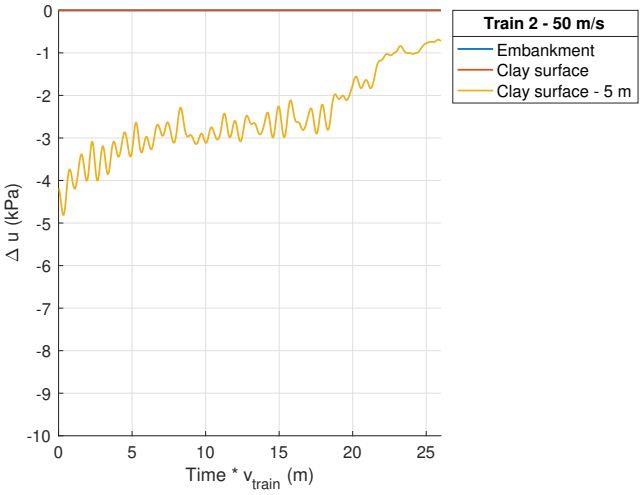

(d) *Train 2:* $v_{train} = 50\,\mathrm{m\,s^{-1}}$.

Figure 3.16: Δu *for train 1 (before cycle 1) & train 2 (after cycle 100k);* $x = 49\,\mathrm{m}$*; with stiffness degradation in model.*

3.4.3 $x = 51\,\mathrm{m}$

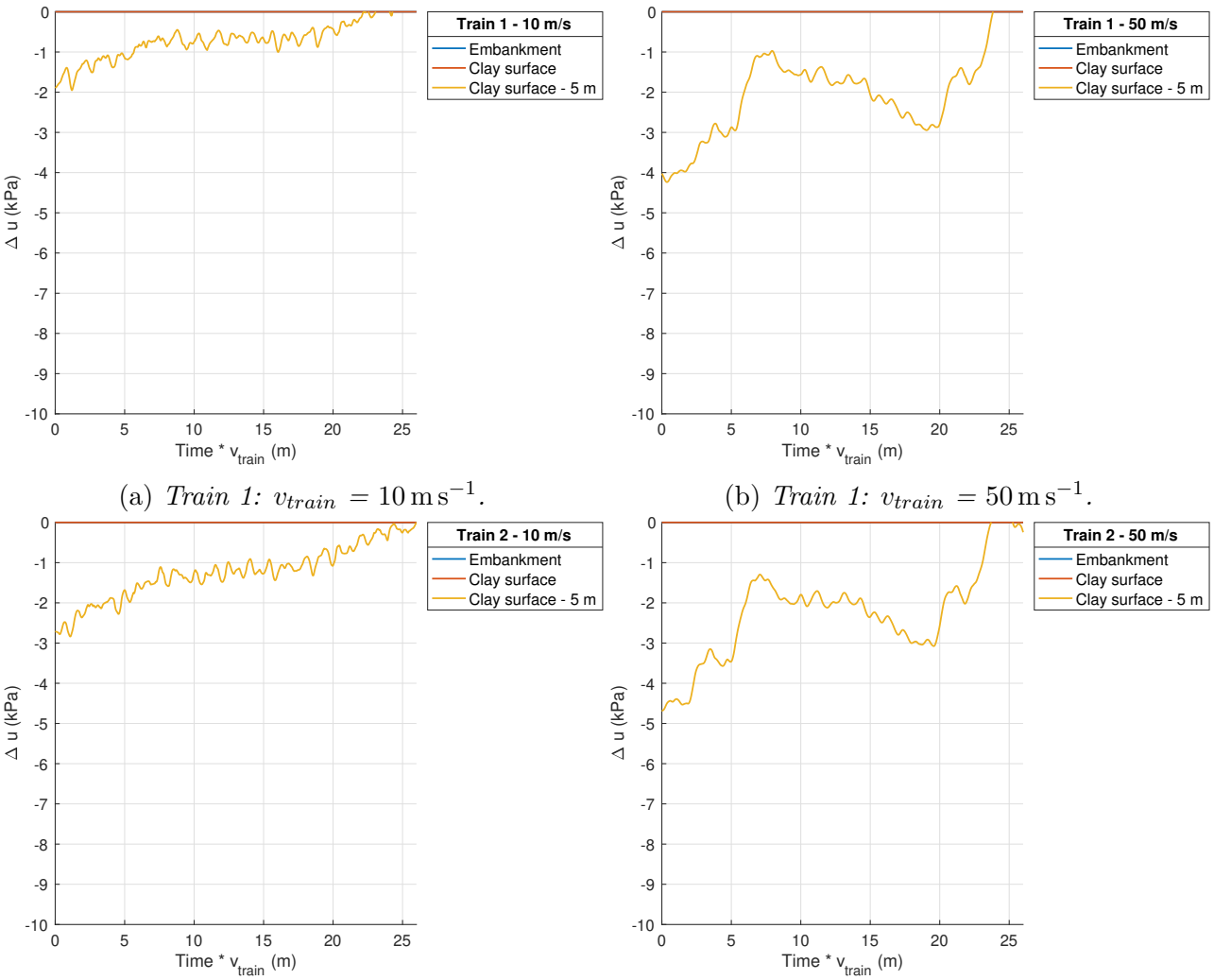

(a) *Train 1:* $v_{train} = 10\,\mathrm{m\,s^{-1}}$.

(b) *Train 1:* $v_{train} = 50\,\mathrm{m\,s^{-1}}$.

(c) *Train 2:* $v_{train} = 10\,\mathrm{m\,s^{-1}}$.

(d) *Train 2:* $v_{train} = 50\,\mathrm{m\,s^{-1}}$.

Figure 3.17: Δu *for train 1 (before cycle 1) & train 2 (after cycle 100k);* $x = 51\,\mathrm{m}$*; no stiffness degradation in model.*

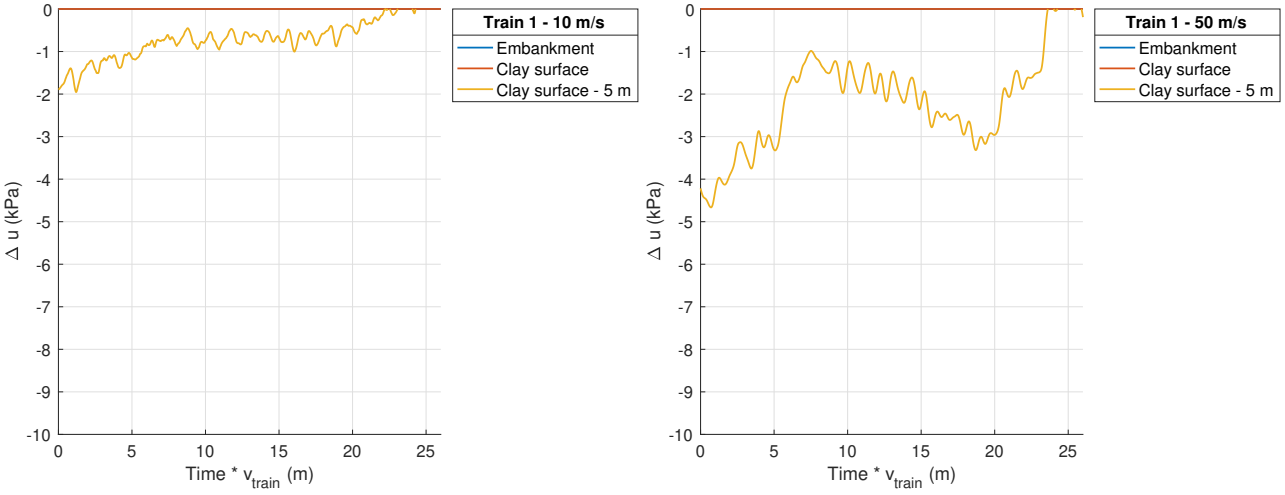

(a) *Train 1:* $v_{train} = 10\,\mathrm{m\,s^{-1}}$.

(b) *Train 1:* $v_{train} = 50\,\mathrm{m\,s^{-1}}$.

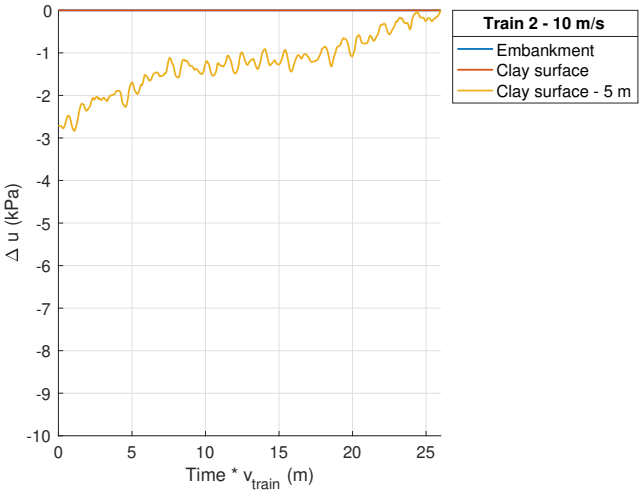

(c) *Train 2:* $v_{train} = 10\,\mathrm{m\,s^{-1}}$.

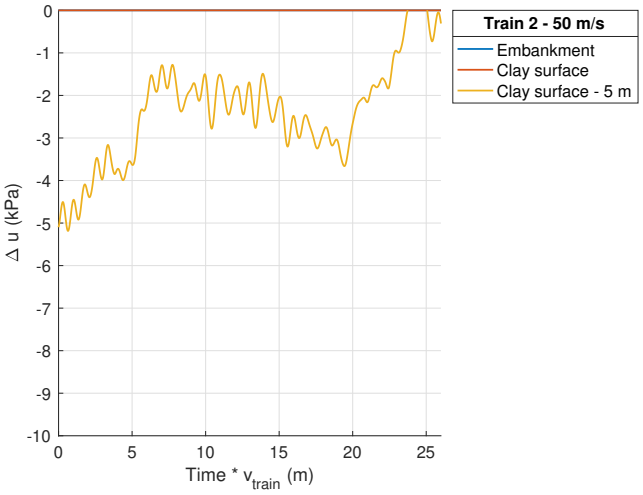

(d) *Train 2:* $v_{train} = 50\,\mathrm{m\,s^{-1}}$.

Figure 3.18: Δu *for train 1 (before cycle 1) & train 2 (after cycle 100k);* $x = 51\,\mathrm{m}$*; with stiffness degradation in model.*

3.5 Normalised vertical accelerations $\frac{a}{g}$

3.5.1 $x = 25\,\mathrm{m}$

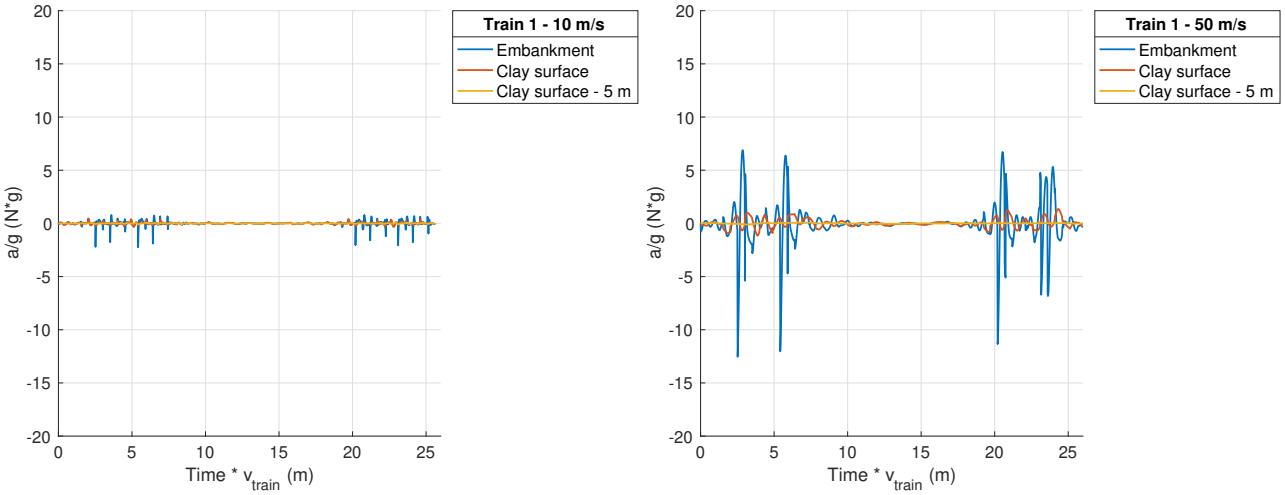

(a) *Train 1:* $v_{train} = 10\,\mathrm{m\,s^{-1}}$.

(b) *Train 1:* $v_{train} = 50\,\mathrm{m\,s^{-1}}$.

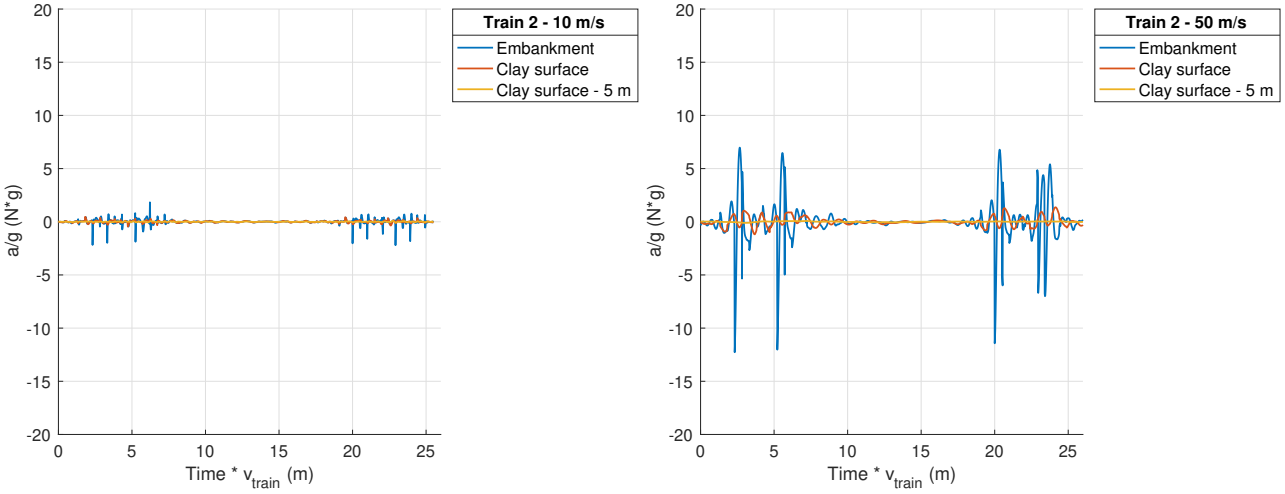

(c) *Train 2:* $v_{train} = 10\,\mathrm{m\,s^{-1}}$.

(d) *Train 2:* $v_{train} = 50\,\mathrm{m\,s^{-1}}$.

Figure 3.19: $\frac{a}{g}$ *for train 1 (before cycle 1) & train 2 (after cycle 100k);* $x = 25\,\mathrm{m}$*; no stiffness degradation in model.*

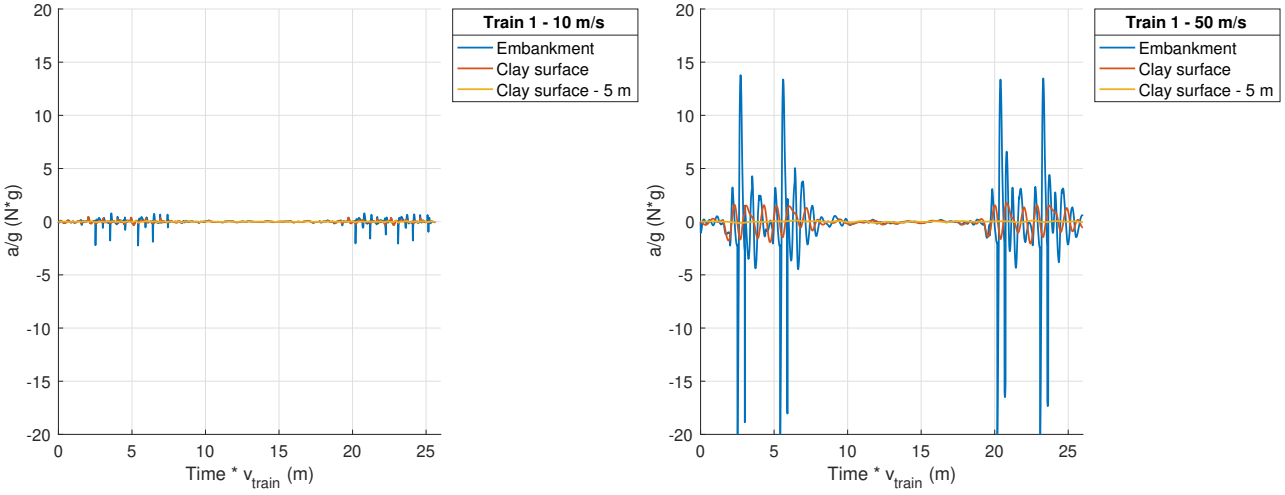

(a) *Train 1:* $v_{train} = 10\,\mathrm{m\,s^{-1}}$.

(b) *Train 1:* $v_{train} = 50\,\mathrm{m\,s^{-1}}$.

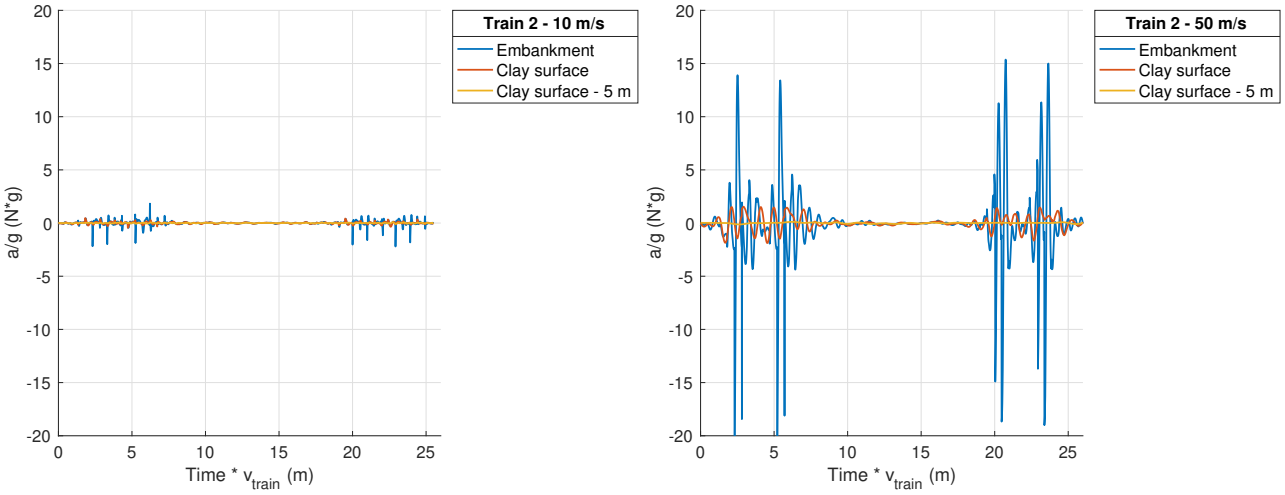

(c) *Train 2:* $v_{train} = 10\,\mathrm{m\,s^{-1}}$.

(d) *Train 2:* $v_{train} = 50\,\mathrm{m\,s^{-1}}$.

Figure 3.20: $\frac{a}{g}$ *for train 1 (before cycle 1) & train 2 (after cycle 100k);* $x = 25\,\mathrm{m}$*; with stiffness degradation in model.*

3.5.2 $x = 49\,\mathrm{m}$

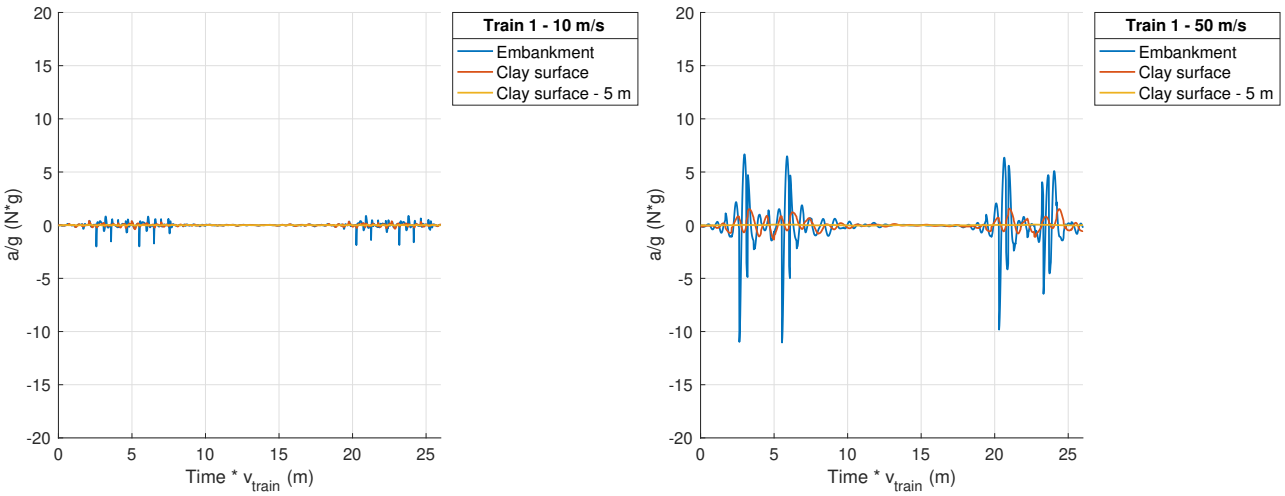

(a) *Train 1:* $v_{train} = 10\,\mathrm{m\,s^{-1}}$.

(b) *Train 1:* $v_{train} = 50\,\mathrm{m\,s^{-1}}$.

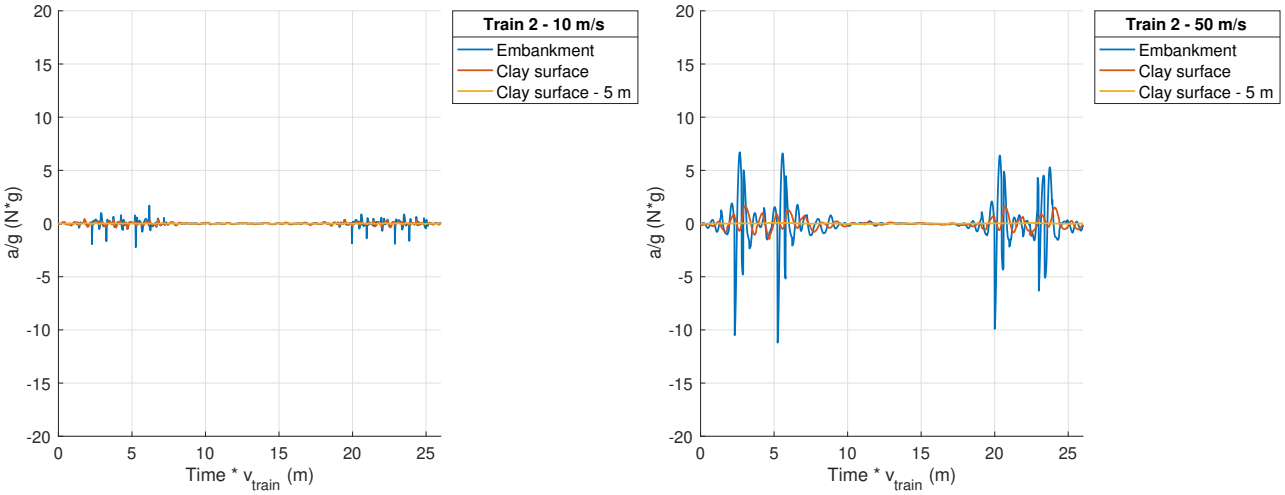

(c) *Train 2:* $v_{train} = 10\,\mathrm{m\,s^{-1}}$.

(d) *Train 2:* $v_{train} = 50\,\mathrm{m\,s^{-1}}$.

Figure 3.21: $\frac{a}{g}$ *for train 1 (before cycle 1) & train 2 (after cycle 100k);* $x = 25\,\mathrm{m}$*; no stiffness degradation in model.*

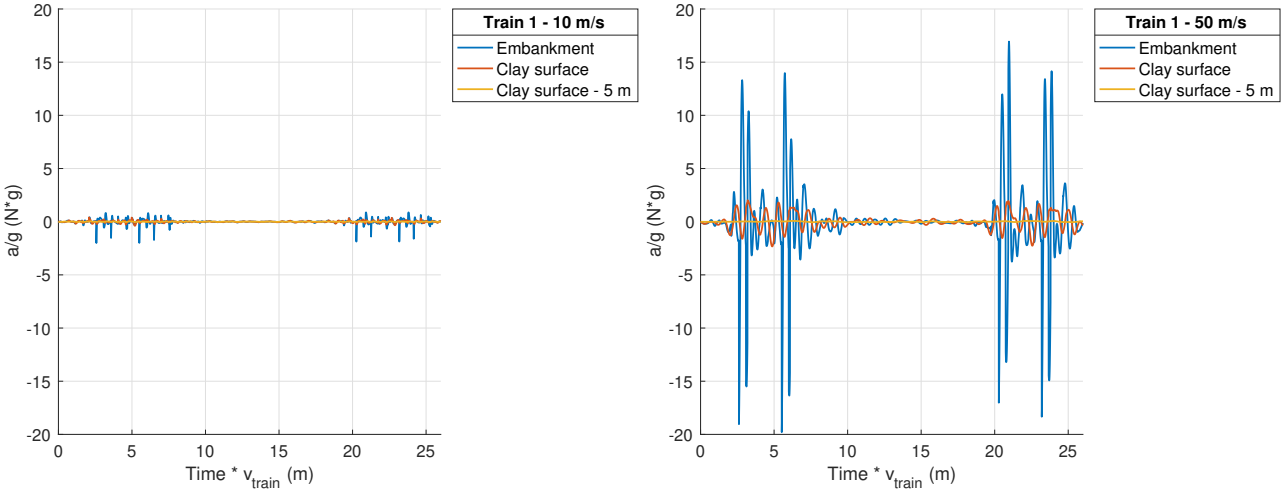

(a) *Train 1:* $v_{train} = 10\,\mathrm{m\,s^{-1}}$.

(b) *Train 1:* $v_{train} = 50\,\mathrm{m\,s^{-1}}$.

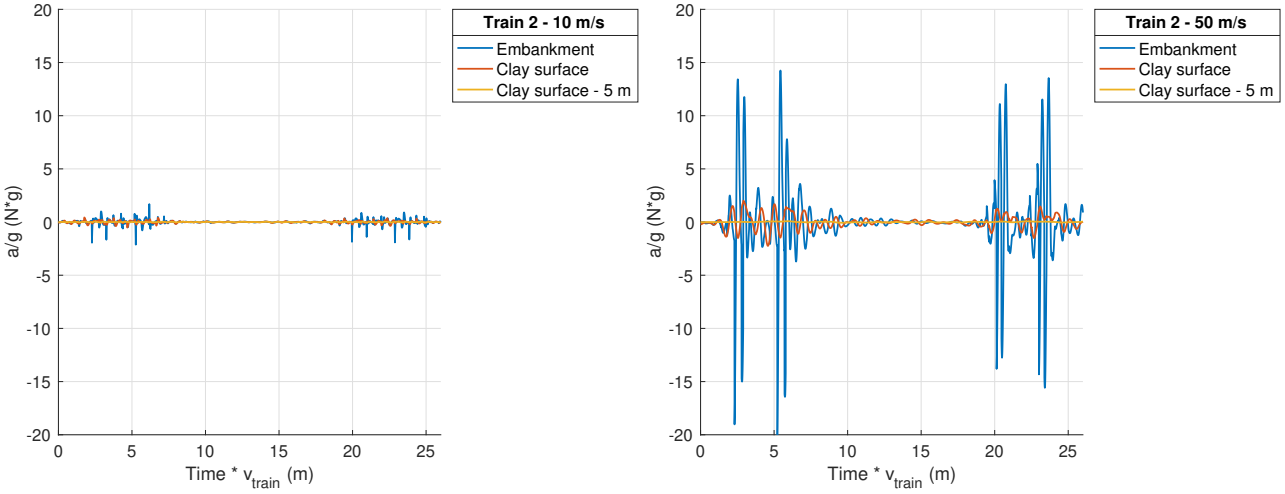

(c) *Train 2:* $v_{train} = 10\,\mathrm{m\,s^{-1}}$.

(d) *Train 2:* $v_{train} = 50\,\mathrm{m\,s^{-1}}$.

Figure 3.22: $\frac{a}{g}$ *for train 1 (before cycle 1) & train 2 (after cycle 100k);* $x = 49\,\mathrm{m}$*; with stiffness degradation in model.*

3.5.3 $x = 51\,\mathrm{m}$

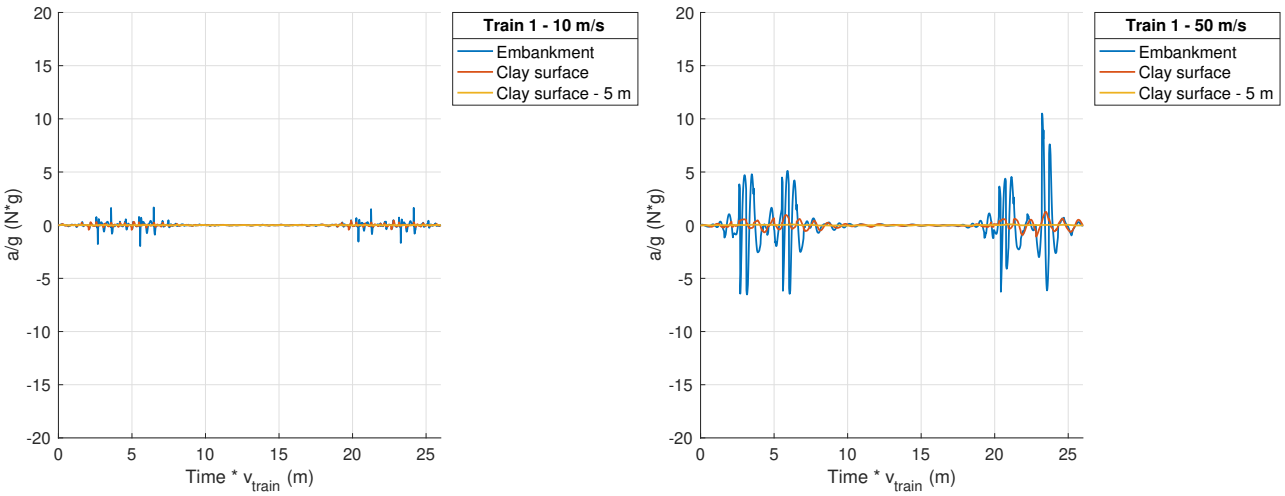

(a) *Train 1:* $v_{train} = 10\,\mathrm{m\,s^{-1}}$.

(b) *Train 1:* $v_{train} = 50\,\mathrm{m\,s^{-1}}$.

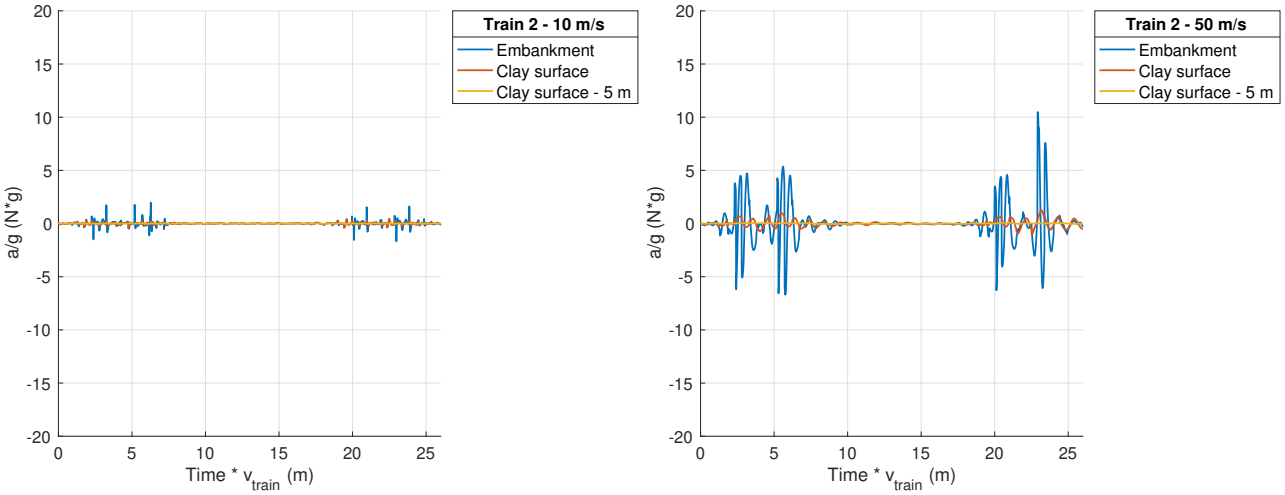

(c) *Train 2:* $v_{train} = 10\,\mathrm{m\,s^{-1}}$.

(d) *Train 2:* $v_{train} = 50\,\mathrm{m\,s^{-1}}$.

Figure 3.23: $\frac{a}{g}$ *for train 1 (before cycle 1) & train 2 (after cycle 100k);* $x = 51\,\mathrm{m}$*; no stiffness degradation in model.*

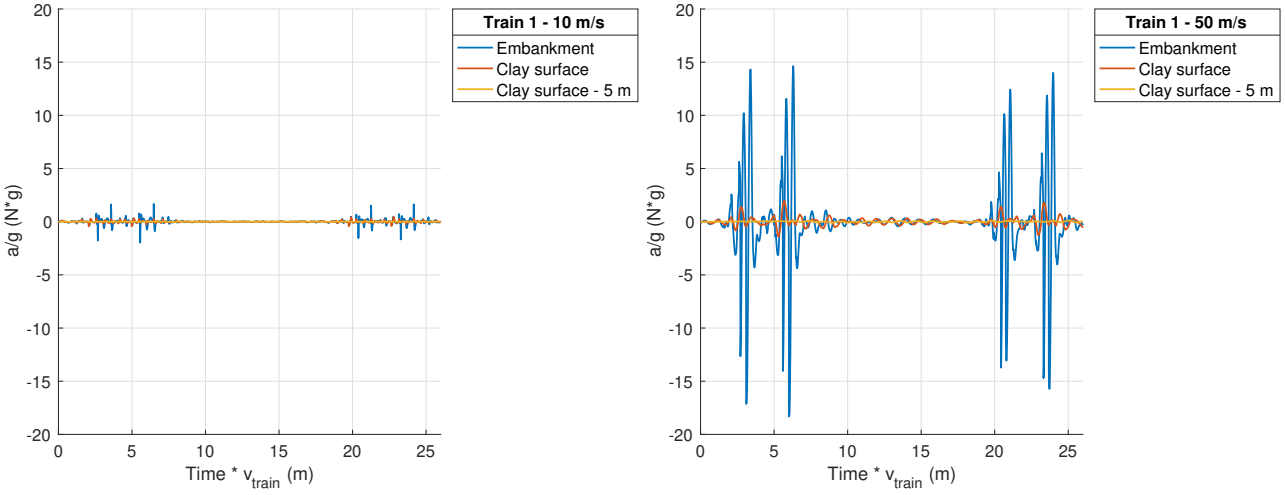

(a) *Train 1:* $v_{train} = 10\,\mathrm{m\,s^{-1}}$.

(b) *Train 1:* $v_{train} = 50\,\mathrm{m\,s^{-1}}$.

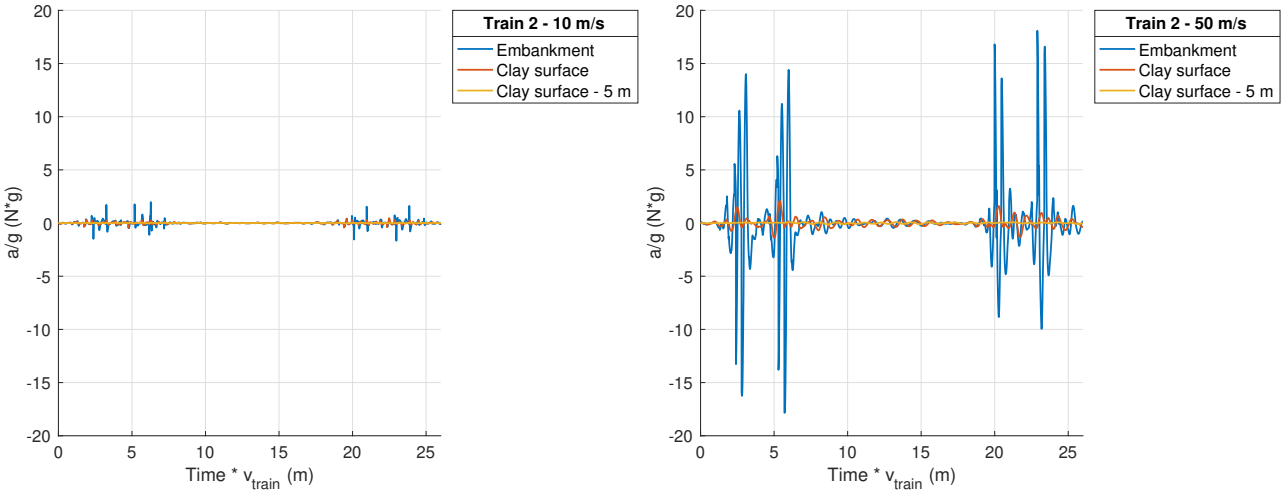

(c) *Train 2:* $v_{train} = 10\,\mathrm{m\,s^{-1}}$.

(d) *Train 2:* $v_{train} = 50\,\mathrm{m\,s^{-1}}$.

Figure 3.24: $\frac{a}{g}$ *for train 1 (before cycle 1) & train 2 (after cycle 100k);* $x = 51\,\mathrm{m}$*; with stiffness degradation in model.*

3.6 Result Interpretation

When studying the results, the following observations are made:

- The cyclic accumulation stage (difference in response between train 1 & train 2) is largest for Δq, the largely undrained response for both train passages does not affect $\Delta p'$ to the same extent. For the current cyclic accumulation amplitude of $q_{max} = 10\,\mathrm{kPa}$ and 100 000 cycles the differences between the passage of train 1 and train 2 are the most substantial for the slow train $v_{train} = 10\,\mathrm{m\,s^{-1}}$;

- The increase in train velocity v_{train} increases the accelerations observed at the surface of the embankment sevenfold, however the magnitude of the accelerations in the subsoil although increasing with train velocity, are benign. Consequently, the change in effective stress generated in the soil reduces with increasing train velocity. A larger part of the external load is dissipated by inertia;

- The effect of stiffness degradation in the model formulation is largest for $v_{train} = 50\,\mathrm{m\,s^{-1}}$. This, however, can be expected: by linking the pseudo-elastic stiffness degradation to a non-linear parameter (destructuration χ) no large effects will be seen in absence of irreversible strains;

- The excess pore water pressure generation is mostly quasi-static, future research should study if this is a model artefact or not. Please note that only the post point 5 m below the surface has water filled pores (the post point at the clay surface has a zero pressure prescribed from the water table);

- In the current simulations the clay near the transition zone at $x = 49\,\mathrm{m}$ has larger accelerations and lower effective stress amplitudes than in the far field $x = 25\,\mathrm{m}$. Furthermore, the excess pore water pressures are drained more effectively;

- The complexity of the modelling approach requires a more systematic study of the interplay between the cyclic accumulation, stiffness degradation and the moving train load.

4 Conclusions & Recommendations

4.1 Conclusions

The report proposes an extension of the recently developed cyclic accumulation model Creep-Sclay1Sc for the incorporation of the degradation of the pseudo-elastic stiffness as function of the destructuration based on experimental data. In addition, a numerical method for modelling moving train loads at boundary value level has been devised. Finally, the non-trivial mapping of the effects of a dynamic event associated to a moving train into cyclic accumulation parameters for the Creep-Sclay1Sc model has been developed.

The newly developed numerical tools have been used to model a transition of a railway embankment from a soft clay that is susceptible to cyclic degradation to a stiff soil. The analyses have highlighted the effect of the train velocity on the dynamic response prior and after 100 000 cycles. The reduction in peak deviatoric and mean effective stress levels was largest for the slow train with $v_{train} = 10\,\mathrm{m\,s^{-1}}$. Furthermore, for both train velocities the behaviour in the soil near the transition was markedly difference from the far field response with larger accelerations and simultaneously smaller increments in effective stress. Finally, the effect of stiffness degradation as implemented in the model does not appreciably change the calculation results, as the magnitude of irreversible strains (hence the amount of destructuration) remains low.

4.2 Recommendations

This research is only a second step towards a full comprehension and modelling capability of the long-term changes in the dynamic response of railway embankments under cyclic loading. The following research activities need to be considered next:

- Establish an experimental link between *cyclic* accumulation of strain and the dynamic soil properties (stiffness and damping);
- Investigate the source of numerical stability of the constitutive model for non-homogeneous distributions of q_{max} in conjunction with complex problem geometries;
- Systematic sensitivity analyses on transition zones for a larger number of transition geometries, loading conditions and soil properties. Care should be taken, however, to only study physical permissible scenarios where the properties and initial conditions in the soil are in equilibrium with the problem geometry.

References

Coelho, B., P. Hölscher, J. Priest, W. Powrie, and F. Barends (2011). An assessment of transition zone performance. *Proc. of the Institution of Mechanical Engineers, Part F: Journal of Rail and Rapid Transit* **225**.2, 129–139.

Dahlberg, Tore (2001). Some railroad settlement models?a critical review. *Proceedings of the Institution of Mechanical Engineers, Part F: Journal of Rail and Rapid Transit* **215**.4, 289–300.

Dijkstra, J., W. Broere, and O.M. Heeres (2011). Numerical simulation of pile installation. *Computers and geotechnics* **38**.5, 612–622.

Gras, J.P., N. Sivasithamparam, M. Karstunen, and J. Dijkstra (2017). Strategy for consistent model parameter calibration for soft soils using multi-objective optimisation. *Computers and Geotechnics* **90**, 164–175. ISSN: 0266-352X. DOI: https://doi.org/10.1016/j.compgeo.2017.06.006.

Karg, C., S. François, W. Haegeman, and G. Degrande (2010). Elasto-plastic long-term behavior of granular soils: Modelling and experimental validation. *Soil Dynamics and Earthquake Engineering* **30**.8, 635–646. ISSN: 0267-7261. DOI: http://dx.doi.org/10.1016/j.soildyn.2010.02.006.

Karstunen, M., H. Krenn, S. Wheeler, M. Koskinen, and R. Zentar (2005). Effect of Anisotropy and Destructuration on the Behavior of Murro Test Embankment. *International Journal of Geomechanics* **5**.2, 87–97.

Leroueil, S. and P.R. Vaughan (1990). The general and congruent effects of structure in natural soils and weak rocks. *Géotechnique* **40**.3, 467–488.

Li, X., M. Ekh, and J.C.O. Nielsen (2016). Three-dimensional modelling of differential railway track settlement using a cycle domain constitutive model. *International Journal for Numerical and Analytical Methods in Geomechanics* **40**.12, 1758–1770.

Mrŏz, Z., V.A. Norris, and O.C. Zienkiewicz (1978). An anisotropic hardening model for soils and its application to cyclic loading. *International Journal for Numerical and Analytical Methods in Geomechanics* **2**.3, 203–221.

Ni, J., B. Indraratna, X. Geng, J. Carter, and Y. Chen (2014). Model of Soft Soils under Cyclic Loading. *International Journal of Geomechanics* **15**.4, 1–10. DOI: 10.1061/(ASCE)GM.1943-5622.0000411.

Nielsen, Jens CO and Xin Li (2018). Railway track geometry degradation due to differential settlement of ballast/subgrade–Numerical prediction by an iterative procedure. *Journal of Sound and Vibration* **412**, 441–456.

Niemunis, A., T. Wichtmann, and Th. Triantafyllidis (2005). A high-cycle accumulation model for sand. *Computers and Geotechnics* **32**.4, 245–263. ISSN: 0266-352X. DOI: http://dx.doi.org/10.1016/j.compgeo.2005.03.002.

Park, C.B., R.D. Miller, and J. Xia (1999). Multichannel analysis of surface waves. *Geophysics* **64**.3, 800–808.

Pasten, C., H. Shin, and J. Santamarina (2014). Long-Term Foundation Response to Repetitive Loading. *Journal of Geotechnical and Geoenvironmental Engineering* **140**.4, 1–11.

Powrie, William, Louis Le Pen, David Milne, and David Thompson (2019). Train loading effects in railway geotechnical engineering: Ground response, analysis, measurement and interpretation. *Transportation Geotechnics* **21**, 100261.

Sato, Y. (1997). "Optimization of track maintenance work on ballasted track". *proceedings of the World Congress on Railway Research (WCRR?97)*, pp. 405–411.

Sivasithamparam, N., M. Karstunen, and P. Bonnier (2015). Modelling creep behaviour of anisotropic soft soils. *Computers and Geotechnics* **69**, 46–57. ISSN: 0266-352X.

Suiker, A.S.J. and R. de Borst (2003). A numerical model for the cyclic deterioration of railway tracks. *International Journal for Numerical Methods in Engineering* **57**.4, 441–470. ISSN: 1097-0207. DOI: 10.1002/nme.683.

Wheeler, S. J., A. Näätänen, M. Karstunen, and M. Lojander (2003). An anisotropic elastoplastic model for soft clays. *Canadian Geotechnical Journal* **40**.2, 403–418. DOI: 10.1139/t02-119.

Wood, T. (2016). "On the Small Strain Stiffness of Some Scandinavian Soft Clays and Impact on Deep Excavations". PhD thesis. Ph. D. thesis, Chalmers University of Technology.

Zuada Coelho, Bruno and Michael A Hicks (2016). Numerical analysis of railway transition zones in soft soil. *Proceedings of the Institution of Mechanical Engineers, Part F: Journal of Rail and Rapid Transit* **230**.6, 1601–1613.